Shedding light on the bluff body wake instability

by

Renzo Trip

March 2016 Technical Reports from Royal Institute of Technology KTH Mechanics SE-100 44 Stockholm, Sweden

Akademisk avhandling som med tillstånd av Kungliga Tekniska Högskolan i Stockholm framlägges till offentlig granskning för avläggande av teknologie doktorsexamen fredag den 8 april 2016 kl 10:15 i sal D2, Lindstedtsvägen 5, Kungliga Tekniska Högskolan, Stockholm.

TRITA-MEK 2016:04 ISSN 0348-467X ISRN KTH/MEK/TR-16/04-SE ISBN 978-91-7595-893-4

©Renzo Trip 2016 Universitetsservice US-AB, Stockholm 2016 Renzo Trip 2016, Shedding light on the bluff body wake instability Linné Flow Centre, KTH Mechanics, SE-100 44 Stockholm, Sweden

Abstract The flow around a vehicle, for example, results in a large resistance and can generate a complex swirl pattern behind the body of the vehicle, which can lead to strong alternating lateral forces. There is therefore a clear need for more fundamental understanding of the instability of this so-called wake region, which arises behind bluff bodies. In this thesis, the focus lies on the relation between the wake inlet conditions and the wake characteristics of a bluff body. This relation is studied experimentally, in the Reynolds number range $2.9 \times 10^3 - 5.5 \times 10^4$. The experiments are carried out in a specially designed test-section, which comprises a rectangular forebody with a smooth leading edge and a blunt trailing edge. The perforated top and bottom surface of this body allow for boundary layer modification by means of wall suction.

Hot-wire an emometry and pressure measurements show that wall suction, in the order of 1% of the free-stream velocity, leads to a significant change of the boundary-layer properties; the boundary-layer thickness decreases and the wall-shear stress increases. Laminar boundary layers take the form of the asymptotic suction boundary layer and turbulent boundary layers are shown to relaminarize, when subject to wall suction above a critical value. A modification of the boundary layer leads to an increase of the vortex shedding frequency and a decrease of the base pressure. Empirical relations for the Strouhal number and the base pressure coefficient are derived. The boundary layer conditions are included in these relations and as result, they hold for both laminar and turbulent boundary layers.

Two-dimensional velocity fields, obtained by means of particle image velocimetry, reveal the effect of boundary-layer modification on the near-wake topology. By dividing the velocity component into (i) mean, (ii) periodic and (iii) random contributions, it can be shown that the confluence point moves upstream, the curvature of streamlines enclosing the trailing edge increases, and the Reynolds normal and shear stresses increase.

The experimental study is continued by introducing interference elements in the wake. The qualitative effect of a splitter plate on the wake characteristics is not altered by boundary-layer modification, but the critical splitter plate length and gap width for which the vortex shedding frequency is suppressed do change. A sensitivity map is obtained experimentally by placing a control rod at various locations in the wake. Considering all limitations of such an experiment, it was found to be in good agreement with the result of a linear stability analysis carried out on the measured mean velocity field.

Descriptors: Bluff body, asymptotic suction boundary layer, vortex shedding, wall suction, particle image velocimetry, flow control, splitter plate, control cylinder

Renzo Trip 2016, En experimentell studie om vakinstabiliteten bakom en trubbig kropp

Linné Flow Centre, KTH Mekanik, SE - 100 44 Stockholm, Sverige

Sammanfattning Strömningen kring exempelvis ett fordon medför ett stort motstånd och kan alstra komplicerade virvelmönster bakom fordonets kropp, vilket kan leda till växelvis starka sidokrafter. Det finns därför ett tydligt behov av ökad grundläggande förståelse för instabiliteten av så kallade vakar, som uppstår bakom trubbiga kroppar. I denna avhandling ligger fokus på sambandet mellan gränsskiktets hastighetsfördelning över en trubbig kropp och dess vaks karaktäristik. Experiment har utförts på en specialdesignad trubbig kropp i Reynolds tal området $2.9 \times 10^3 - 5.5 \times 10^4$. Kroppen är en tjock plan platta med en strömlinjeformad framkant och en tvär bakkant. Över- och undersidan av kroppen är perforerade vilket möjliggör gränsskiktsmodifieringar genom väggsugning.

Varmtrådsmätningar och tryckmätningar visar att väggsugning i storleksordningen 1% av friströmshastigheten har en stor inverkan på gränsskiktets utformning; tjockleken minskar och väggskjuvspänningen ökar. Laminära gränsskikt tar formen av det asymptotiska sugningsgränsskiktet, och turbulenta gränsskikt kan relaminariseras när sugningen överskrider ett kritiskt värde. Väggsugning ökar virvelavkastningsfrekvensen samtidigt som bastrycket i vaken minskar. Empiriska relationer baserade på gränsskiktstjockleken och hastighetsprofilens formfaktor har erhållits för både Strouhal talet och bastryckskoefficienten. Valet att inkludera gränsskiktsparametrar i relationerna medför att dessa samband gör sig gällande oavsett om gränsskikten är laminära eller turbulenta.

Två-dimensionella hastighetsfält har mätts upp med particle image velocimetry för att påvisa gränsskiktsmodifieringens effekt på vakens topologi nära kroppen. Genom att dela upp hastighetskomponenterna i (i) medel, (ii) periodiska och (iii) turbulenta bidrag ser man att vakens konfluenspunkt förflyttar sig uppströms, kurvaturen av strömlinjen som omsluter bakkanten ökar och Reynolds normal- och skjuvspänningar ökar.

Vidare har den experimentella studien bestått i att undersöka effekten av interfererande element i vaken. Den kvalitativa effekten av en splitterplatta på vakens karaktäristik påverkas inte av gränsskiktsmodifieringar, även om både den kritiska längden och luckan (mellan bakkanten till plattans start) ändras, för när virvelavkastningen upphör. En experimentell kartläggning över vakens sensitivitet för placering av en stav i vaken har även utförts i kontrollsyfte. God överensstämmelse med numeriska resultat har erhållits där både linjär stabilitets- och sensitivitetsanalys på de uppmätta hastighetsfälten genomförts.

Deskriptorer: trubbig kropp, asymptotiska sugnings- gränsskiktet, virvelavkastning, väggsugning, particle image velocimetry, flödeskontroll, splitterplatta, kontrollstav

Preface

This doctoral thesis within the area of fluid mechanics concerns an experimental study on the wake behind a rectangular forebody with variable inlet conditions. The thesis is divided into two parts. The first part gives an introduction, discussing: the relevance of the research, the underlying fluid mechanics and the experimental methodology. A summary of the results and conclusions presented in the second part is also included. The second part consists of seven papers that are redacted to meet the present thesis format.

March 2016, Stockholm Renzo Trip



Contents

Abstra	act	iii
Prefac	re	v
Chapt	er 1. Introduction	1
Chapt	er 2. Bluff body wakes	3
2.1.	The Kármán vortex street	3
2.2.	Vortex formation region	4
2.3.	Wake inlet conditions	5
2.4.	Far wake region	6
Chapt	er 3. Boundary layers	7
3.1.	Previous Studies	7
3.2.	Boundary layer approximation	8
3.3.	Falkner-Skan boundary layer	10
3.4.	Asymptotic suction boundary layer	11
3.5.	Turbulent boundary layer	12
3.6.	Turbulent suction boundary layer	14
Chapt	er 4. Experimental setup and measurement techniques	16
4.1.	Rectangular forebody with perforated surfaces	16
4.2.	Hot-wire anemometry	18
4.3.	Pressure measurements	21
4.4.	Particle Image Velocimetry	24
4.5.	Sorting PIV images	26
4.6.	Vortex detection	30
Chapt	er 5. Summary of results	33
5.1.	Boundary layer properties	33

5.2. Wake characteristics	36
5.3. Near wake topology	39
5.4. Total, periodic and random velocity component	40
Chapter 6. Conclusions	44
Chapter 7. Papers and authors contributions	46
Chapter 8. Acknowledgements	49
References	51
Paper 1. A new test section for wind tunnel studies on wake instability and its control	e 65
Paper 2. An experimental study on the wake of a rectangular forebody with suction applied over the surfaces	r 105
Paper 3. Boundary layer modification by means of wall suctio and the effect on the wake behind a rectangular forebody	n 119
Paper 4. An experimental study on the relation between the wake inlet conditions and the near wake topology	e 149
Paper 5. On the effect of boundary layer modification on the near wake topology of a rectangular forebody	e 159
Paper 6. An experimental study on the combined effect of boundary layer modification and a splitter plate of the wake characteristics	n 199
Paper 7. Investigation of passive control of the wake past a thick plate by stability and sensitivity analysis of experimental data	

$\begin{array}{c} {\bf Part\ I} \\ {\bf Overview\ and\ summary} \end{array}$

CHAPTER 1

Introduction

Let's start with a little experiment, for which only a sheet of paper is required. Fold the top two corners to the middle of the paper and do the same with the resulting flaps. Fold the paper in half and finish your airplane by folding back the two wings. Launching this streamlined body will show that it cuts through the air swiftly. The small resistance, or drag, on the body is mainly due to thin boundary layers developing over the surfaces.

Now, firmly crumple the same piece of paper into a wad of approximately spherical proportions. The aerodynamics of this altered configuration flying through the air is very different. A wake will form behind this so-called 'bluff body', because the boundary layer will now separate from the body, and as a result the drag will increase.

The above experiment, illustrated in figure 1.1, demonstrates that a bluff body can be defined as a non-aerodynamic body, which is characterized by a low base pressure and the formation of a wake region when in relative motion to the fluid surrounding it. For cylindrical bodies, the wake is typically dominated by large scale vortices periodically shed from either side of the body.

Bluff bodies are found in various internal flow applications and as structures subject to an external flow. Vortex shedding can be used to enhance mixing and the predictability of the vortex shedding frequency is conveniently exploited in vortex flow meters. But the same phenomenon must also be taken into consideration when designing, for example, bridges, chimneys or skyscrapers. These type of elongated structures can suffer from vortex shedding induced vibrations, especially when the vortex shedding frequency is close to the structural natural frequency. Furthermore, bluff bodies are associated with acoustical noise and the pressure drag leads to increased fuel consumption of, e.g., road vehicles.

The widespread occurrence of bluff bodies may explain the large amount of related research. In general, the flow around a bluff body is well understood, i.e. in terms of flow topology and stability. However, the relation between the wake inlet conditions, comprising the body geometry and the boundary layer prior to separation, and the wake characteristics is still relatively unknown. The aim of this thesis is to increase the knowledge on this relation by adding to the sparse amount of available experimental data.

1

2 1. INTRODUCTION

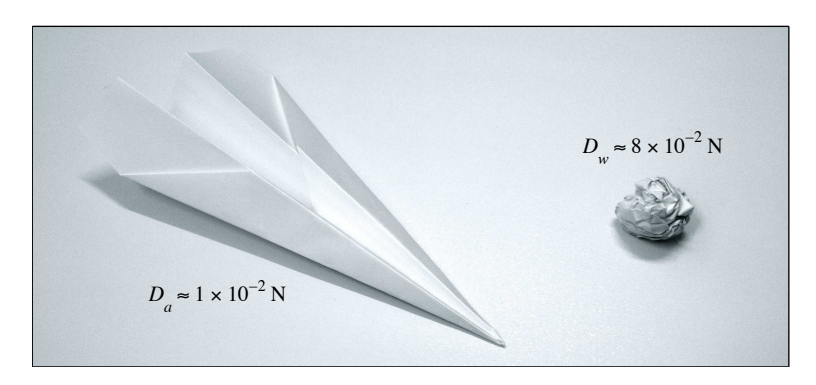


FIGURE 1.1. Estimation of the drag on a paper airplane (D_a) and on the same sheet of A4-paper crumpled into a wad (D_w)

A specially designed setup will be used, that allows for boundary layer modification by means of wall-suction over the flat surfaces of rectangular fore-body. The laminar and in particular the turbulent boundary layer over a flat plate subject to uniform wall-suction are relatively untouched topics themselves. Therefore, after having introduced the bluff body wake in chapter 2, the unique features of the asymptotic suction boundary layer and some characteristics of a turbulent boundary subject to wall-suction will be discussed in chapter 3. In chapter 4, the experimental setup and the employed measurement techniques are described. A selection of results is presented in chapter 5, followed by a summary of the main conclusions in chapter 6. The first part of the thesis is completed with an overview of the papers collected in the second part of the thesis.

CHAPTER 2

Bluff body wakes

In the previous chapter, the bluff body was characterized by the wake that forms behind it when in relative motion to a fluid. Cylindrical bluff bodies experience a relatively large drag force, and are subject to vibrations. In this chapter, the origin of these characteristics is discussed, and the wake inlet conditions are introduced. Finally, the fluid dynamics 'far' away from the body is considered.

2.1. The Kármán vortex street

The sound produced by objects swinging rapidly through the air and by air currents over stretched wires, lead to the pioneering work of Strouhal (1878). By spinning circular rods of various materials and length around at a constant velocity in a kind of centrifuge, the inverse proportionality between the diameter of the rod h and the the ratio between the frequency f and the velocity U was found:

$$St_h = \frac{fh}{U} , \qquad (2.1)$$

where the constant St is nowadays referred to as the Strouhal number. Strouhal (1878) observed that St varied with temperature, which lead Rayleigh (1878) to conclude that the Strouhal number should be a function of the Reynolds number, which is given by:

$$Re_h = \frac{Uh}{\nu} , \qquad (2.2)$$

with ν the kinematic viscosity.

Von Kármán & Rubach (1912) concluded on the basis of a stability analysis that the flow behind a bluff body can be described by a 'vortex street' consisting of two rows of asymmetrically placed vortices of opposite vorticity. In addition, Von Kármán & Rubach (1912) noted that the vortices must originate from the boundary layers developing over the surface of the body, a concept introduced by Prandtl (1904) several years earlier.

The Von Kármán vortex street is the result of a self-exited oscillation (Monkewitz 1988). The critical Reynolds number for the onset of the (global) absolute instability was found to be $Re \approx 47$ for a circular cylinder (Provansal et al. 1987) and values up to $Re \approx 120$ have been reported for bodies with a blunt trailing edge (Buresti 2012). The instability is a result of the interaction

4 2. BLUFF BODY WAKES

between the two shear layers separating from the body (Abernathy & Kronauer 1962), which implies that the low base pressure is a consequence and not the cause of the vortex shedding (Strykowski & Sreenivasan 1990).

Considering the canonical case of a circular cylinder, the wake is characterized by laminar vortices, periodically shed from the top and bottom surface of the body for $47 \le Re \le 150$. In the range $150 \le Re \le 350$, the laminar periodic wake undergoes a transition to turbulence, whereby the point of transition moves upstream for increasing Re until the eddies become turbulent upon formation. For $3.5 \times 10^2 \le Re \le 2 \times 10^5$, referred to as the subcritical or transition-in-shear layer regime, the laminar shear layers that have separated from the body undergo a transition to turbulence. And at even higher Reynolds number the boundary layers prior to separation become turbulent. A detailed description of the different flow regimes is available in the literature (Roshko 1953; Norberg 1994; Williamson 1996; Zdravkovich 1997).

2.2. Vortex formation region

The base pressure and the vortex shedding frequency are determined in a region immediately behind the body, where the vortices are formed. The description of the Kármán vortex street by Von Kármán & Rubach (1912) does not provide a relation between these properties and the origin of the vortices.

An early attempt to find this relation was made by Fage & Johansen (1927), who conducted a series of experiments by hot-wire anemometry on an inclined plate. Fage & Johansen (1927) reported that the frequency increases as the inclination, and hence, the distance between the separating shear layers, decreases. A universal Strouhal number was formulated by Roshko (1954) based on the the distance between the the separating shear layers and a characteristic wake velocity, but noted that this formulation would probably not be valid for all Reynolds numbers. The shortening of the vortex formation region for increasing Reynolds number, within the subcritical regime (Schiller & Linke 1933; Bloor 1964), was identified as an effect of key importance to formulate the mechanics of the formation region (Gerrard 1966; Berger & Wille 1972).

The formation of vortices from alternating sides of a body is a process in which a vortex on one side draws fluid, bearing vorticity of opposite sign, across the wake from the other side (Gerrard 1966). The initial vortex is fed by circulation from the connected shear layer, and hence, the vortex radius increases until the supply is cut off by the initialized vortex (Bearman 1965). The fluid drawn across the wake is partly entrained into the growing initial vortex, into the shear layer and into the near wake region in between the growing vortex and the base.

The amount of fluid entrained by the shear layer depends on the length of the turbulent shear layer. When the point of transition of the shear layer moves closer to the body, the entrainment by the shear layer is increased. Because the entrained fluid is bearing vorticity of the opposite sign, the strength of the shear layer is reduced (Anderson & Szewczyk 1997). As a result, a weaker vortex is formed, and the reversed flow is reduced leading to a shorter formation region. A shorter formation region is associated with a higher shedding frequency.

The shear layer thickness at the end of the formation region was identified as another major factor in the vortex formation mechanism (Gerrard 1966). When the shear layer is thicker it takes longer for sufficient vorticity of the opposite sign to be entrained and initiate the shedding of the vortex, and hence, the shedding frequency is lower. Hence, the two major factors in the formation of vortices have opposite effect on the shedding frequency.

The shear layer thickness is a function of the free-stream turbulence and the boundary conditions of the flow along the body (Berger & Wille 1972). The boundary layer growing over the body should therefore be considered to explain changes in the vortex shedding frequency and the base pressure (Hoerner 1965).

2.3. Wake inlet conditions

The trailing edge details and the boundary layers on the top and bottom side prior to separation comprise the wake inlet conditions. A modification of the wake inlet conditions can significantly change the wake characteristics. For example, increasing the corner radius of the trailing edge, the extrema being a square and circular cylinder, leads to an increase of the vortex shedding frequency (Hu et al. 2006; Taylor et al. 2011). In case the trailing edge is blunt, and hence, the separation of the boundary layers is fixed at the sharp corners, the wake inlet conditions can be varied by modifying the boundary layers developing over the body.

Although the importance of the boundary layer prior to separation was recognized, the available research on the topic is sparse. A change of the boundary layer state, from laminar to turbulent, was found to induce a reduction of the vortex shedding frequency for both a circular and a squared trailing edge (Sieverding & Heinemann 1990). Petrusma & Gai (1994) showed that the base pressure of a blunt trailing edge airfoil is a function of the ratio between the base height to the separating boundary layer momentum thickness. An increase of the base pressure and a reduction of the vortex shedding frequency for an increase of the boundary layer thickness was also reported by Rowe et al. (2001). The increase in base pressure has been ascribed to a greater shedding organization and a weaker vortex strength associated with a thicker boundary layer (Durgesh et al. 2013). Similar results have been presented for asymmetric bodies (Mariotti & Buresti 2013). In all studies here mentioned, the boundary layer thickness was modified by means of roughness elements mounted on or in close proximity to the body.

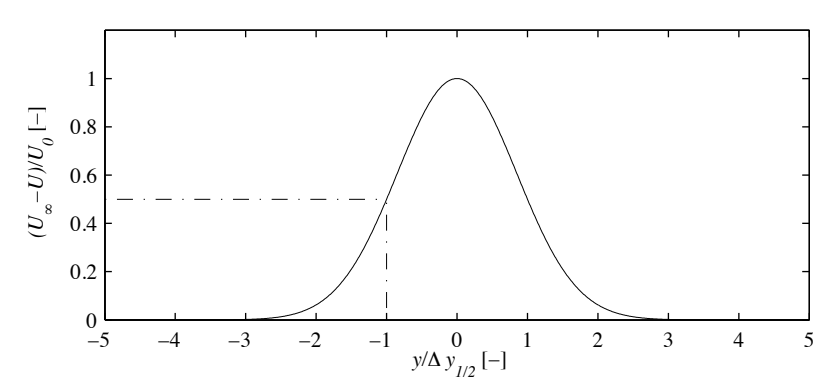


FIGURE 2.1. The mean far wake velocity profile (eq. 2.5), with $y_{1/2}$ the half-wake width and U_0 the velocity deficit.

2.4. Far wake region

It is well known that the wake eventually 'forgets' about its origin and approaches a self-similar state with increasing downstream position. The self-similar state is reached in what is called the far wake, corresponding to x/h > 30 (Antonia & Rajagopalan 1990).

To describe the mean velocity profile in the far wake the velocity deficit U_0 :

$$U_0(x) \equiv U_{\infty} - U(x,0) ,$$
 (2.3)

and the half wake width $\Delta y_{1/2}$:

$$U(x, \Delta y_{1/2}) = U_{\infty} - \frac{1}{2}U_0(x) , \qquad (2.4)$$

are defined, where U_{∞} is the free-stream velocity, see figure 2.1. Taking the thin shear layer equation as a starting point, and introducing an eddy viscosity model with a constant turbulent viscosity, it can be shown that the mean velocity profile is given by (Pope 2000):

$$U(x,y) = U_{\infty} - U_0(x) \exp\left[-\ln(2)\left(\frac{y}{\Delta y_{1/2}}\right)^2\right].$$
 (2.5)

The momentum loss implied by the velocity deficit is proportional to the total drag acting on the body. The drag is defined as the force component in the direction of motion. The forces acting on a body can, based on their origin, be divided into (skin-) friction forces and pressure forces. The friction forces act tangential to the surface. Accordingly, the drag can be divided into the friction drag, also called viscous drag, and pressure drag, which is also referred to as form drag. The total drag on an aerodynamic, or streamlined, body is dominated by the viscous drag, whereas the pressure drag is typically much larger for bluff bodies.

CHAPTER 3

Boundary layers

The aim of this study is to analyze the wake flow topology and its characteristics when the wake is subject to different inlet conditions. In order to do so, a rectangular forebody with a perforated surface that allows for modification of the boundary layer by means of blowing and/or suction is used. A detailed description is given in Paper 1. In this chapter, a description of laminar and turbulent boundary layers with and without wall-suction will be given.

3.1. Previous Studies

The idea to modify the boundary layer by means of suction was first discussed in the 1930s as a way to improve the aerodynamics of airplane wings. The advantage of suction in this context is twofold: a thinner boundary layer leads to a reduction of the induced wake, and the skin friction is likely to be reduced if the transition to turbulence of the initially laminar boundary layer is postponed or even prevented.

Griffith & Meredith (1936) showed that an exact analytical solution exist for the laminar boundary layer over a flat plate with a uniform suction velocity, V_0 , applied over the surface. For this so called Asymptotic Suction Boundary Layer (ASBL), the growth of the boundary layer is opposed by the velocity component in the direction of the wall, with the result that the streamwise velocity U(y) through the boundary layer is no longer a function of the streamwise position x. Here, y is the wall-normal coordinate to the body surface. The continuity equation then dictates that the wall-normal velocity must be constant. As the name suggest, the boundary layer asymptotes towards the ASBL state, and hence, is achieved only sufficiently far downstream.

A numerical solution of the boundary layer with uniform suction over a plate in a state before the ASBL is established is given by Iglish (1944), with suction starting at the leading edge of the plate, and Rheinboldt (1955), with suction starting after an initial entry length. A complete overview of the theory of laminar flow over a flat plate with uniform suction can be found in Rosenhead (1963).

Kay (1948) was the first to show experimentally that the velocity profile does indeed approach the ASBL when uniform suction is applied over the surface of a flat plate. The ASBL could only be established and retained if the boundary layer was laminar at the start of the suction region, i.e. after an initial non-porous entry length. No conclusive evidence for the existence of an equivalent turbulent asymptotic boundary layer could be given for an initially turbulent boundary layer. However, it was shown that suction does lead to a considerable thinning of the turbulent boundary layer.

A comprehensive experimental study on the existence of a turbulent asymptotic suction boundary layer (TASBL) was carried out by Dutton (1958). For a critical ratio V_0/U_∞ a turbulent asymptotic suction profile exists, but no general asymptotic solution was found. The critical ratio depends on the state of the boundary layer at commencement of suction and the surface type: porous or perforated. For values smaller or greater than this critical value there was no tendency, at least not within the length of the plate, for the boundary layer to reach a state in which the boundary layer thickness and the profile shape remained constant. When suction is increased, the velocity profile shape divides into two distinct parts, an inner part which resembles the laminar asymptotic suction profile and an outer layer which takes the form of a long thin tale which only slowly diminishes. A numerical study by Bobke et al. (2016) showed that the TASBL can not be reached under practical experimental conditions. A conclusion that was disputed by recent experimental efforts, which suggest that a turbulent asymptotic state can be reached under specific condions in a windtunnel¹.

It has been shown both theoretically (Fransson & Alfredsson 2003), numerically (Schlatter & Örlü 2011; Khapko 2014) and experimentally (Fransson 2010; Yoshioka $et\ al.\ 2004$) that wall suction suppresses the disturbance growth and may significantly delay or inhibit the break down to turbulence. Dutton (1958) suggested that the boundary layer might eventually relaminarize and reach the laminar asymptotic state.

Two approaches can be distinguished in regard of describing the turbulent boundary layer subject to wall suction: those based on Prandtl's mixing length theory (Rotta 1970; Simpson 1970) and the ones that seek for similarity laws for the inner and outer region with a common overlap region (Black & Sarnecki 1958; Tennekes 1965). The latter is only valid for moderate levels of suction and for turbulent boundary layers that are in equilibrium state. The first method, on the other hand, was proved by Black & Sarnecki (1958) to be in satisfactory agreement with the experimental results shown by Dutton (1958) and Kay (1948).

3.2. Boundary layer approximation

Based on a scaling analysis of the Navier-Sokes equation the equations of motion can be simplified for the relatively thin boundary layer, see e.g. Kundu & Cohen

¹Private communication, M. Ferro and J. H. M. Fransson, KTH Mechanics, Stockholm, Sweden

(2008). For a steady, two-dimensional, incompressible flow the boundary layer equations (3.6, 3.7) and the continuity equation (3.8) read:

$$U\frac{\partial U}{\partial x} + V\frac{\partial U}{\partial y} = -\frac{1}{\rho}\frac{\partial P}{\partial x} + \nu\frac{\partial^2 U}{\partial y^2}, \qquad (3.6)$$

$$0 = -\frac{\partial P}{\partial y} , \qquad (3.7)$$

$$\frac{\partial U}{\partial x} + \frac{\partial V}{\partial y} = 0 , \qquad (3.8)$$

with the fluid density ρ , the kinematic viscosity ν , the static pressure P and U and V the velocity components in the streamwise x and wall normal y directions, respectively. Equation (3.7) implicates that the pressure is uniform across the boundary layer, i.e. the static pressure at the surface is equal to the static pressure outside the boundary layer. Hence, the pressure gradient can be written in terms of the free stream velocity U_{∞} using the Bernouilli equation as:

$$-\frac{1}{\rho}\frac{dP_{\infty}}{dx} = U_{\infty}\frac{dU_{\infty}}{dx} \ . \tag{3.9}$$

For a boundary layer developing over a solid surface, equations (3.6)–(3.8) has to obey the following boundary conditions:

$$U(x,0) = 0$$
, $U(x,\infty) = U_{\infty}$, $V(x,0) = 0$. (3.10)

The thickness of the boundary layer can be expressed as the displacement thickness δ_1 :

$$\delta_1 = \int_0^\infty \left(1 - \frac{U}{U_\infty} \right) dy , \qquad (3.11)$$

which is defined as the distance by which the surface has to be moved outward in order to get the same mass flux in a hypothetical frictionless flow. Another expression of the boundary layer thickness can be given if one instead considers the momentum loss due to the presence of the boundary layer. The momentum thickness δ_2 is given by:

$$\delta_2 = \int_0^\infty \frac{U}{U_\infty} \left(1 - \frac{U}{U_\infty} \right) dy \ . \tag{3.12}$$

The ratio of the displacement thickness and momentum thickness:

$$H_{12} = \frac{\delta_1}{\delta_2} \,, \tag{3.13}$$

is the shape factor H_{12} of the boundary layer profile.

Hereafter, the laminar boundary layer without suction will be discussed, followed by a discussion on the laminar boundary layer with suction. Thereafter, the equivalent turbulent boundary layers will be described.

3.3. Falkner-Skan boundary layer

Falkner & Skan (1930) showed that equation (3.6) has a similarity solution in case the velocity outside the boundary layer varies in the form:

$$U_{\infty}(x) = ax^n \,\,\,(3.14)$$

with n and a being constants. The similarity variable η corresponds to:

$$\eta = \frac{y}{\delta(x)} = y\sqrt{\frac{U_{\infty}}{x\nu}} = \frac{y}{x}\sqrt{Re_x} , \qquad (3.15)$$

with $\delta(x)$ the boundary layer thickness and Re_x the Reynolds number based on the downstream distance x. If a similarity solution exists, then the velocity distribution U/U_{∞} in the wall normal direction at each location x is given by the same function g:

$$\frac{U}{U_{\infty}} = g(\eta) \ . \tag{3.16}$$

In order to solve the system of equations with the similarity approach, a stream function ψ is introduced, with:

$$U = \frac{\partial \psi}{\partial y} , V = -\frac{\partial \psi}{\partial x} , \qquad (3.17)$$

and which thus obeys the continuity equation (Eq. 3.8). It follows:

$$\psi = \int_0^y U \ dy = \delta \int_0^\eta U \ d\eta = \delta \int_0^\eta U_\infty g(\eta) \ d\eta = \sqrt{\nu x U_\infty} f(\eta) \ , \tag{3.18}$$

where:

$$g(\eta) = \frac{df}{d\eta} \ . \tag{3.19}$$

Substitution of equation (3.14), equation (3.17) and equation (3.18) into equation (3.6) with equation (3.9) gives an ordinary differential equation:

$$f'''(\eta) + \frac{n+1}{2}f(\eta)f''(\eta) - nf'(\eta)^2 = 0 , \qquad (3.20)$$

with boundary conditions:

$$f'(0) = 0$$
, $f'(\infty) = 1$, $f(0) = 0$. (3.21)

Equation (3.21) is the so called Falkner-Skan equation, an equation that can be solved numerically giving a similarity solution of the velocity distribution. Using equation (3.11), the displacement thickness becomes:

$$\delta_{1,\text{FS}} = b\delta(x) , \qquad (3.22)$$

with:

$$b = \frac{\delta_{1,FS}}{\delta(x)} = \int_{\eta=0}^{\eta_{\infty}} (1 - f') d\eta = \eta_{\infty} - f(\eta_{\infty}) .$$
 (3.23)

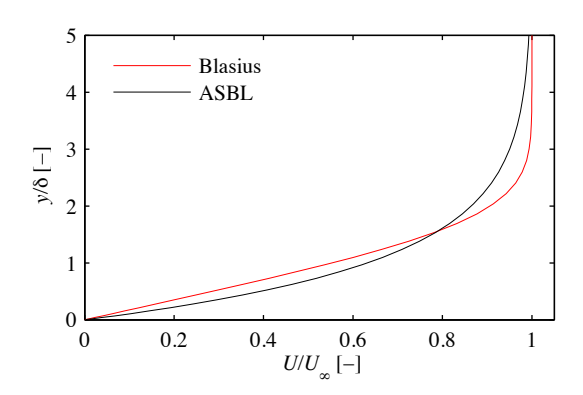


FIGURE 3.1. A comparison of the Blasius boundary layer and the ASBL velocity profile.

3.4. Asymptotic suction boundary layer

Here, the zero-pressure gradient laminar boundary layer with a uniform suction velocity, V_0 , will be considered, starting with an approach of an asymptotic limit of streamwise independence as $x \to \infty$. Sufficiently far downstream the growth of the boundary layer, promoted by the viscosity, is exactly opposed by the negative velocity V(y) in the wall-normal direction. Hence, the boundary layer thickness remains constant and the streamwise velocity U is no longer a function of the streamwise position x. The continuity equation (3.8) then dictates that the wall-normal velocity V_0 must be constant and independent of the wall-normal coordinate y and equation (3.6) becomes:

$$V_0 \frac{dU}{dy} = \nu \frac{d^2U}{dy^2} , \qquad (3.24)$$

with the boundary conditions given by:

$$U(x,0) = 0 , U(x,\infty) = U_{\infty} .$$
 (3.25)

This differential equation can readily be shown to have an analytical solution:

$$\frac{U(y)}{U_{\infty}} = 1 - \exp\left(\frac{yV_0}{\nu}\right) , \qquad (3.26)$$

which is in the exponential form and known as the Asymptotic Suction Boundary Layer (ASBL). In figure 3.1, the ASBL velocity profile is compared to the Blasius boundary layer, which is the zero-pressure gradient Falkner-Skan solution. The boundary layer length scales and the shape factor are given by:

$$\delta_{1,\text{ASBL}} = -\frac{\nu}{V_0} , \ \delta_{2,\text{ASBL}} = -\frac{1}{2} \frac{\nu}{V_0} , \ H_{12,\text{ASBL}} = 2 ,$$
 (3.27)

which are independent of U_{∞} , a unique property further discussed in Paper 2.

The solution of the laminar boundary layer with a zero-pressure gradient and suction applied that has not yet reached the asymptotic state was described by Rheinboldt (1955). A similar variable substitution as shown for the Falkner-Skan solution can be made to find similarity. However, an additional similarity variable ξ is needed:

$$\xi = V_0 \sqrt{\frac{x}{U_\infty \nu}} , \eta = y \sqrt{\frac{U_\infty}{x\nu}} . \tag{3.28}$$

Again, a stream function is introduced similar to equation (3.18), but it is now a function, f, of ξ and η :

$$\psi = \sqrt{\nu x U_{\infty}} f(\xi, \eta) . \tag{3.29}$$

Substitution of equation (3.29) using equation (3.17) into equation (3.6) with the pressure gradient equal to zero gives:

$$\frac{\partial^3 f}{\partial \eta^3} + \frac{1}{2} f \frac{\partial^2 f}{\partial \eta^2} + \frac{1}{2} \xi \left[\frac{\partial f}{\partial \xi} \frac{\partial^2 f}{\partial \eta^2} - \frac{\partial f}{\partial \eta} \frac{\partial^2 f}{\partial \eta \partial \xi} \right] , \tag{3.30}$$

with the boundary conditions:

$$f'(\xi,0) = 0$$
, $f'(\xi,\infty) = 1$, $f(\xi,0) = \xi$. (3.31)

In order to solve this equation, the boundary layer is progressively calculated for points downstream of an initial position, typically the position where suction is commenced. The corresponding value of ξ_0 is given by:

$$\xi_0 = V_0 \sqrt{\frac{x_0}{U_\infty \nu}} ,$$
 (3.32)

with x_0 corresponding to the entry length from the start of boundary layer to the initial point where suction is applied. The displacement thickness $\delta_{1,RB}$ is given by:

$$\frac{\delta_{1,\text{RB}}}{\delta(x)} = \int_{\eta_0}^{\eta_\infty} (1 - f') d\eta = \eta_\infty - f(\xi, \eta_\infty) + f(\xi, \eta_0) . \tag{3.33}$$

3.5. Turbulent boundary layer

The boundary layer undergoes a natural transition to turbulence, when the Reynolds number $Re_x \approx 5 \times 10^5$, with Re_x given by:

$$Re_x = \frac{U_{\infty}x}{\nu} , \qquad (3.34)$$

where x is the distance from the leading edge. The analysis found in most books about turbulent boundary layers, is based on the division of the turbulent boundary into two regions: the inner region where the turbulent stresses are negligible compared to the viscous stresses and the outer region where the viscous stresses are negligible compared to the turbulent stresses. The inner and outer layers have different characteristic length scales. The outer layer, similar to the laminar boundary layer, scales with the boundary layer thickness

 δ . The inner layer, on the other hand, scales with the viscous length scale ν/u_{τ} , with u_{τ} being the friction velocity given by:

$$u_{\tau} = \sqrt{\tau_w/\rho}$$
 , where $\tau_w = \mu \frac{\partial U}{\partial y}\Big|_{y=0}$, (3.35)

and τ_w is the wall shear stress. The scaled velocity can consequently be described by the functions $\Phi(y^+)$ and $\Psi(Y)$:

Inner region:
$$U^+ = \frac{U}{u_\tau} = \Phi(\frac{yu_\tau}{\nu}) = \Phi(y^+)$$
, (3.36)

Outer region:
$$\frac{U_{\infty} - U}{u_{\tau}} = \Psi(\frac{y}{\delta}) = \Psi(Y) , \qquad (3.37)$$

which are referred to as the law of the wall and the velocity defect law, respectively. The inner and outer region overlap for large enough Reynolds numbers. Within this overlap region both laws must hold. The derivative of equation (3.36) and equation (3.37) multiplied with y yields the following expression:

$$\frac{1}{u_{\tau}}\frac{\partial U}{\partial y} = y^{+}\frac{d\Phi}{dy^{+}} = -Y\frac{d\Psi}{dY} = \text{const.} , \qquad (3.38)$$

which must be constant because the two relations on the right depend on different length scales. As a result, the velocity profile must be logarithmic in this overlap region:

$$u^{+} = \frac{1}{\kappa} \ln y^{+} + C_{1} , \qquad (3.39)$$

$$u^{+} = \frac{1}{\kappa} \ln y^{+} + C_{1} , \qquad (3.39)$$

$$\frac{U_{\infty} - U}{u_{\tau}} = \frac{1}{\kappa} \ln Y + C_{2} , \qquad (3.40)$$

with κ being the Von Kármán constant and C_1 and C_2 other arbitrary constants.

A self-similar equation can be found starting with the equation of motion, as was done for the laminar cases. However, the flow properties are time dependent now, due to the turbulent fluctuations. By applying Reynolds decomposition, decomposing the instantaneous flow properties into mean and fluctuating components $(U = \bar{u} + u')$, the turbulent boundary layer equation can be derived:

$$\bar{u}\frac{\partial \bar{u}}{\partial x} + \bar{v}\frac{\partial \bar{u}}{\partial y} = -\frac{1}{\rho}\frac{\partial \bar{p}}{\partial x} + \nu\frac{\partial^2 \bar{u}}{\partial y^2} - \frac{\partial}{\partial y}\left(\overline{u'v'}\right) , \qquad (3.41)$$

$$0 = -\frac{\partial \bar{p}}{\partial y} , \qquad (3.42)$$

and the continuity equation reads:

$$\frac{\partial \bar{u}}{\partial x} + \frac{\partial \bar{v}}{\partial y} = 0 \tag{3.43}$$

Due to the additional Reynolds stress term $\overline{u'v'}$ there is no solution to this set of equations, unless a turbulence model is used to express it in terms of the mean velocity field.

The Prandtl mixing length is such a turbulence model. It assumes that lumps of fluid retain their momentum while being displaced by large eddies over distance l_m , referred to as the mixing length. Then the velocity fluctuations u'(y) and v'(y) can be written as:

$$u'(y) \sim v'(y) \sim l_m \frac{\partial \bar{u}}{\partial y}$$
, (3.44)

and consequently:

$$-\overline{u'v'} \sim l_m^2 \left(\frac{\partial \bar{u}}{\partial u}\right)^2 . \tag{3.45}$$

The mixing length l_m is assumed to be proportional to the distance from the wall with the Von Kármán constant κ , introduced earlier, as the proportionality constant:

$$l_m = \kappa y \ . \tag{3.46}$$

Within the overlap region, where the turbulent stress is approximately equal to the wall shear stress ρu_{τ}^2 , one obtains:

$$\frac{u_{\tau}}{\kappa y} = \frac{\partial \bar{u}}{\partial y} \,\,\,\,(3.47)$$

which can readily be shown to yield the same logarithmic velocity distribution found by the two layer approach. The Prandtl mixing length model is nowadays considered to be obsolete, but has proved to work rather well (Davidson 2004). The reason it is introduced here, is the lack of an equivalent two layer approach for the turbulent boundary layer with suction. As will be shown in the next section, Prandtl's mixing length model allows for a good description.

The logarithmic velocity distribution within the overlap region can be extended to hold in the outer layer and the viscous sublayer by adding a wake function and applying an appropriate damping function, respectively. Such an example for a so called composite velocity profile can be found in Nickels (2004) for example.

3.6. Turbulent suction boundary layer

To describe the turbulent boundary layer with suction, the theory by Rotta (1970) is followed, starting with the turbulent boundary layer equations and the continuity equation (see equations 3.41 to 3.43). For the asymptotic suction boundary layer the derivatives of the mean flow quantities with respect to x are rendered zero. Although an asymptotic state might not be reached for the turbulent suction boundary layer, it is assumed that these terms will be

relatively small and can therefore be neglected. Integrating the remaining terms of equation (3.41) leads to:

$$\nu \frac{d\bar{u}}{dy} - \overline{u'v'} = u_{\tau}^2 + V_0 \bar{u} , \qquad (3.48)$$

where the invoked boundary layer conditions, which are similar to those stated in equation (3.10), lead to the additional wall shear stress term on the right hand side.

To be able to solve this equation, the previously discussed Prandtl's mixing length model is introduced, i.e. equation (3.45) and equation (3.46). To include the viscous sublayer, the van Driest damping function is applied (Van Driest 1956), leading to:

$$-\overline{u'v'} = \kappa^2 y^2 \left[1 - \exp\left(-y \frac{\sqrt{u_\tau^2 + V_0 \overline{u}}}{\nu A}\right) \right]^2 \left(\frac{\partial \overline{u}}{\partial y}\right)^2 , \qquad (3.49)$$

with A being the van Driest constant. Upon substitution of equation (3.49) into equation (3.48) one will recognize a quadratic equation which can readily be shown by invoking the quadratic formula to give:

$$\frac{d\bar{u}}{dy} = \frac{2\left(u_{\tau}^2 + V_0 \bar{u}\right)}{\nu + \sqrt{\nu^2 + 4\kappa^2 y^2 \left[1 - \exp\left(-y\sqrt{\left(u_{\tau}^2 + V_0 \bar{u}\right)/(\nu A)}\right)\right]^2 \left(u_{\tau}^2 + V_0 \bar{u}\right)}}, \quad (3.50)$$

which can be solved using a numerical solver.

In the present study, the friction velocity u_{τ} and the wall position y_w are obtained from the experimental data in a least square fit algorithm based on equation (3.50). An initial "guess" of y_w is found by a linear extrapolation of points close to the wall and the empirical ICET skin-friction relation (Bailey et al. 2013) is used to obtain an initial guess of u_{τ} . The van Driest constant and the von Kármán constant are A=26 and $\kappa=0.38$, respectively. Rotta (1970) treats A as a constant, but notes that it is more likely to be a function of the wall suction. Adding it as an additional fit parameter hampered an accurate fit of y_w and u_{τ} and therefore it is treated as constant here as well.

CHAPTER 4

Experimental setup and measurement techniques

Measurements have been carried out in a specially designed setup, which will be introduced here. An elaborate description and evaluation of the setup is the topic of Paper 1. The employed measurement techniques; hot-wire anemometry, pressure measurements, and particle image velocimetry, will be presented, including more advanced analyzing techniques.

4.1. Rectangular forebody with perforated surfaces

In previous studies on the relation between the wake inlet conditions and the wake characteristics, the boundary layer was modified by adding some kind of surface roughness (Sieverding & Heinemann 1990; Petrusma & Gai 1994; Rowe et al. 2001; Durgesh et al. 2013; Mariotti & Buresti 2013). This type of boundary layer modification provides only limited control, and hence, the number of cases is typically small. In addition, the turbulence level is different for the controlled case compared to the uncontrolled case. To overcome these limitations, a method based on boundary layer modification by means of wallsuction will be employed. Modification of the wake inlet conditions by means of transpiration has been applied to circular cylinders (Mathelin et al. 2001a,b: Fransson et al. 2004). A parameter study including the boundary layer properties is complicated for the case of a circular cylinder, due to translocation of the point of separation. Therefore, a bluff body with a blunt trailing edge will be considered here, for which the point of separation is fixed at the sharp corners. In addition, a flat surface allows to measure, in detail, a boundary-layer velocity profile to characterize the wake inlet condition. Something which is much more challenging on a cylinder considering both the curved surface and the relatively thin boundary layer.

A test-section housing a body specially designed to allow for boundary layer modification by means of suction is used. The test-section is an interchangeable component of the Boundary Layer (BL) wind tunnel. The BL-tunnel, of the closed-loop type, is located in the Odqvist Laboratory at KTH Mechanics. For further specifications the interested reader is referred to Lindgren (2002). Here, the main features of the test-section and the body in particular will be discussed.



FIGURE 4.1. Photograph of the test-section situated in the Boundary Layer (BL) wind tunnel.

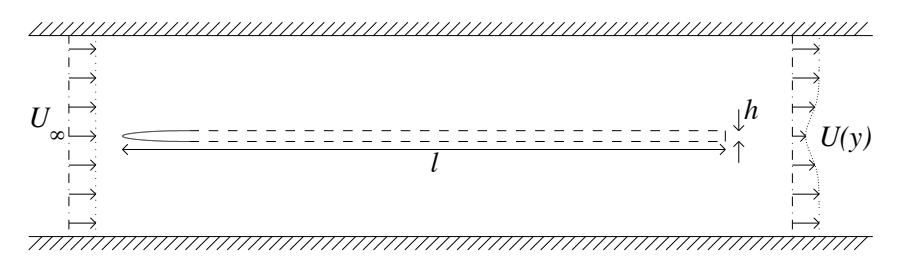


FIGURE 4.2. A schematic side view of the body.

The test-section, shown in figure 4.1, is 4 m long, 0.5 m wide and 0.75 m high. The body is mounted horizontally on the symmetric axis of the test-section. In the description of the body, the term 'forebody' will be used to indicate the part of the body before separation, whereas the part of the body after separation is referred to as the 'base'.

The rectangular forebody is 2 m long and spans the entire test section to produce an essentially two-dimensional flow. For bodies longer than twenty-five body heights, the boundary layer characteristics are insensitive to the leading edge geometry (Parker & Welsh 1983). This statement also holds for even shorter bodies as long as flow separation at the leading edge is prohibited, which is here achieved by fitting a 30 cm long, smooth, elliptical, leading edge. In addition, the streamwise extent of the forebody assures that the boundary layer thickness is significant compared to the body thickness of 4 cm, and, that

the ASBL can be obtained in case wall suction is applied. The blockage ratio based on the body thickness is 5.3%. Below 6%, no effect on the pressure distribution and the vortex shedding frequency is expected, and up to 7% the effect is very small (West & Apelt 1982). Hence, no significant effect is expected here either.

The top and bottom surfaces of the body, which are made of 0.9 mm thick titanium sheets, are perforated to allow for suction and/or blowing. A porosity of 0.5% is obtained with 60 μ m laser drilled holes, that are uniformly distributed across the entire surface. The space between the upper and lower surface is divided into compartments, each connected to an external duct system through the lateral sides of the test section. This construction assures a homogenous pressure drop across the perforated surfaces, when a DC fan is operated at the basis of the duct system. A measure of the wall-normal velocity is obtained by relating the pressure drop to the velocity of the air transpired through the perforations, on the basis of a relation given by Goldstein (1938), which was experimentally verified for the type of surface considered here by Pol et al. (2011). A detailed description of the venting system and the calibration of the wall-normal velocity as function of the pressure drop is given in Paper 1.

4.2. Hot-wire anemometry

The Hot-Wire Anemometry (HWA) technique is based on the forced-convective heat transfer from a heated wire by the flow it is exposed to. How the heat transfer is translated into a measure of the flow velocity depends on type of HWA that is being used. The most obvious procedure, referred to as Constant Current Anemometry (CCA), is to keep the current heating the wire constant and use the change in voltage over wire due to the changing resistance as a measure for the flow velocity. To measure turbulent flow properties it is common to use Constant Temperature Anemometry (CTA), because this alternative allows a high sampling frequency, up to kHz in practice. In the CTA mode the wire temperature is kept constant and the voltage required to do so is used as a measure for the velocity.

The wire is operated at a constant temperature, T_h , that is higher than the ambient temperature to make the sensor less sensitive to temperature fluctuations. Based on the definition:

$$OH = \frac{R(T_h) - R(T_{cal})}{R(T_{cal})},$$
 (4.51)

with R the resistance of the wire and $T_{\rm cal}$ the temperature of the surrounding fluid during calibration. The overheat OH is typically chosen between 0.5 and 0.8, where a higher overheat captures turbulent fluctuations better. For boundary layer measurements a lower overheat is sometimes used, as will be discussed shortly.

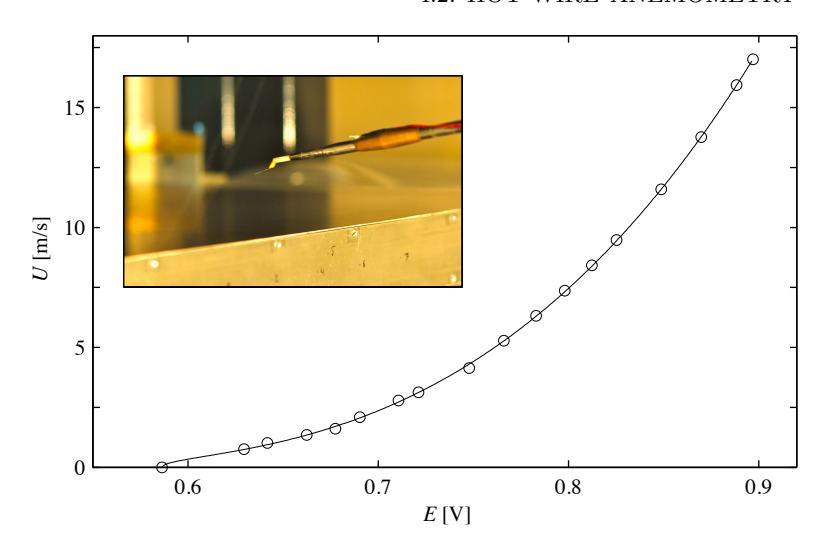


FIGURE 4.3. Typical hot-wire calibration curve. In the inset, the hot-wire probe used for boundary layer measurements is shown.

One relation between the anemometer output voltage E and the velocity U is given by the modified King's law (Johansson & Alfredsson 1982):

$$U = k_1 \left(E^2 - E_0^2 \right)^{\frac{1}{n}} + k_2 \left(E - E_0 \right)^{\frac{1}{2}} , \qquad (4.52)$$

where E_0 is the voltage at U=0 m/s and the coefficients k_1 , k_2 and n are to be found by calibration of the hot-wire against the reading from e.g. a Prandtl tube located in the free stream. An example of a calibration curve is shown in figure 4.3. The designation 'modified' refers to the second term on the right-hand side which is added to account for the effect of free convection. Free convection has a significant contribution at low velocities, for example close to a wall.

In figure 4.3 the in-house made boundary layer hot-wire probe is shown. The hot-wire is typically soldered between two prongs at the extremity of the hot-wire probe. Tungsten and platinum are common materials for the hot-wire, because these metals have a high melting point and their resistance varies linearly with temperature for the temperatures of interest. For increased strength a platinum/rhodium alloy can be used. The diameter of the hot-wire is in the order of micrometers in diameter and has a length to diameter ratio of $l_h/d_h > 200$ so that the heat conduction to the prongs can be neglected.

4.2.1. Near-wall boundary layer measurements

Operating a hot-wire within a boundary layer over a porous surface with suction applied in the wall-normal direction raises the question whether the wall normal

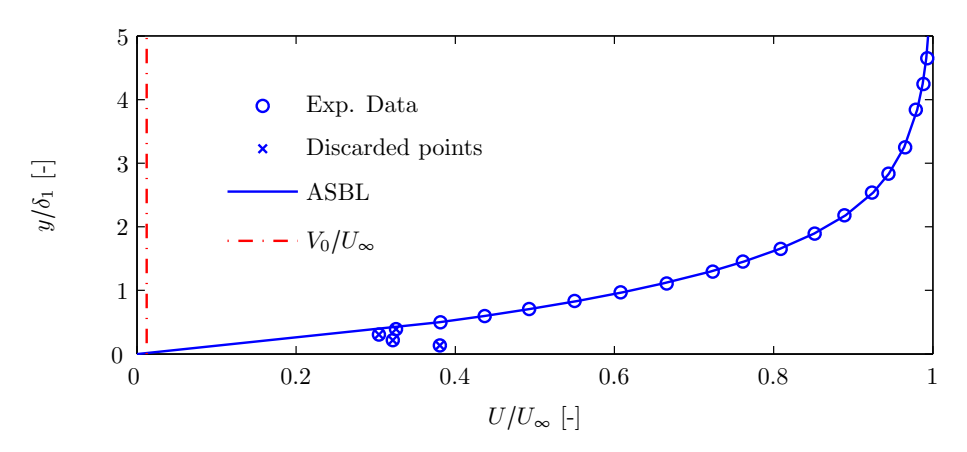


FIGURE 4.4. Boundary layer measurements with a hot-wire ($U_{\infty}=1.0~{\rm m/s},\,v_0/U_{\infty}=0.012$).

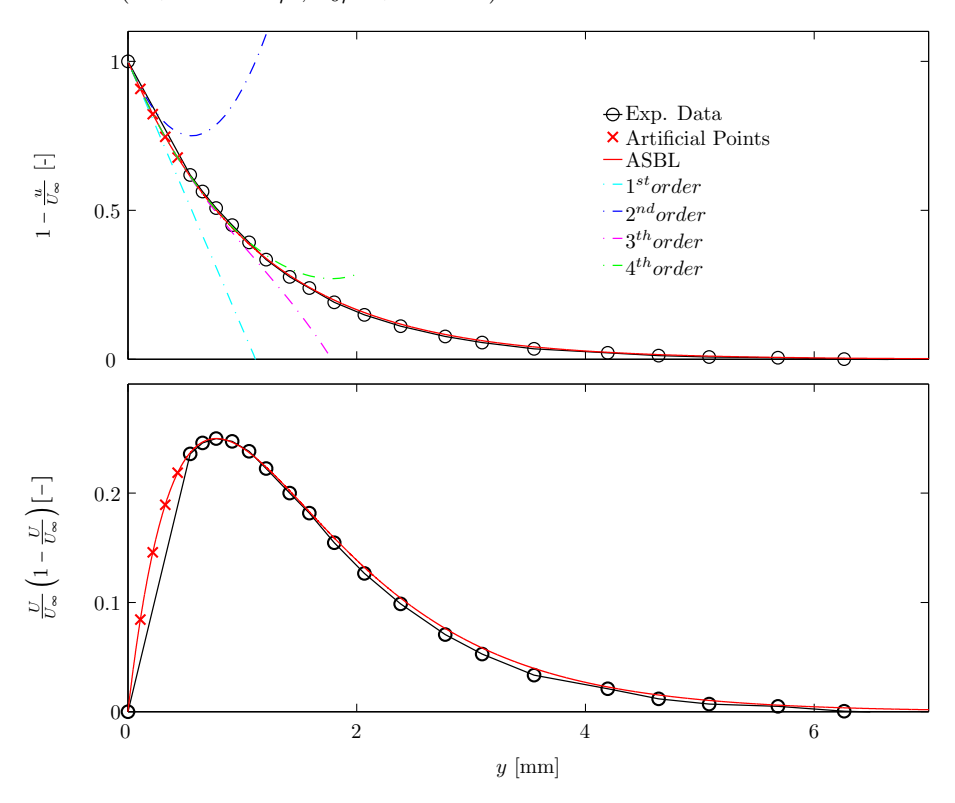


FIGURE 4.5. Displacement and momentum thickness integrand, including the Taylor series expansion.

velocity leads to a significant increase of the forced-convection. Because the wall normal velocity is much smaller than the streamwise velocity component, even close to the wall as indicated in figure 4.4, the additional contribution can be neglected.

Figure 4.4 does show that the velocity is overestimated close to the wall. The overestimation is caused by heat conduction from the hot-wire to the wall, an error that can be minimized by keeping the overheat ratio low. Points from the wall up to the point of minimum velocity are discarded. In addition, one more point is omitted if the velocity derivative has not reached a maximum.

It is apparent that the boundary layer measurements close to the wall are underresolved. This leads to an underestimation of the momentum thickness and to lesser extent to an overestimation of the displacement thickness, see figure 4.5. To improve the estimate of the momentum thickness a Taylor series expansion of the displacement thickness is used to obtain additional artificial points close to the wall in case of the ASBL. For the ASBL, the Taylor series expansion at the wall of the displacement thickness integrand I is given by:

$$I = 1 - \frac{U}{U_{\infty}} = 1 - \left(1 - \exp\left[-\frac{V_0}{\nu}y\right]\right) = \exp\left[-\frac{V_0}{\nu}y\right] , \qquad (4.53)$$

$$I(0) = 1 - \frac{V_0}{\nu} y + \frac{1}{2} \left(\frac{V_0}{\nu}\right)^3 y^3 - \frac{1}{6} \left(\frac{V_0}{\nu}\right)^4 y^4 + O(y^4) . \tag{4.54}$$

It is clear from figure 4.5 that the first four terms will give a proper approximation. The additional artificial points do not lead to a considerable improvement in case of the displacement thickness, but it does show a clear effect for the momentum thickness.

4.2.2. Vortex shedding frequency measurements

A hot-wire is also used to measure the shedding frequency. Although the shedding frequency can be obtained from measurements in the boundary layer or in the wake, a better signal-to-noise ratio can be obtained with a probe placed downstream of the trailing edge just outside the wake, as shown in figure 4.6. The sampling frequency for most measurements is chosen to be $f_s = 3$ kHz, which is more than enough for capturing the shedding frequency considering the Nyquist criterion.

The anemometer offers the possibility to apply a high- and a low- pass filter. The high-pass filter can be used to remove low frequency fluctuations if present, which is not the case in the present wind tunnel. A low-pass filter of 0.3 kHz is used to avoid aliasing and to remove electronic noise.

4.3. Pressure measurements

Pressure measurements typically comprise a Pitot or a Prandtl tube, which are robust compared to the fragile hot-wire probes discussed in the previous

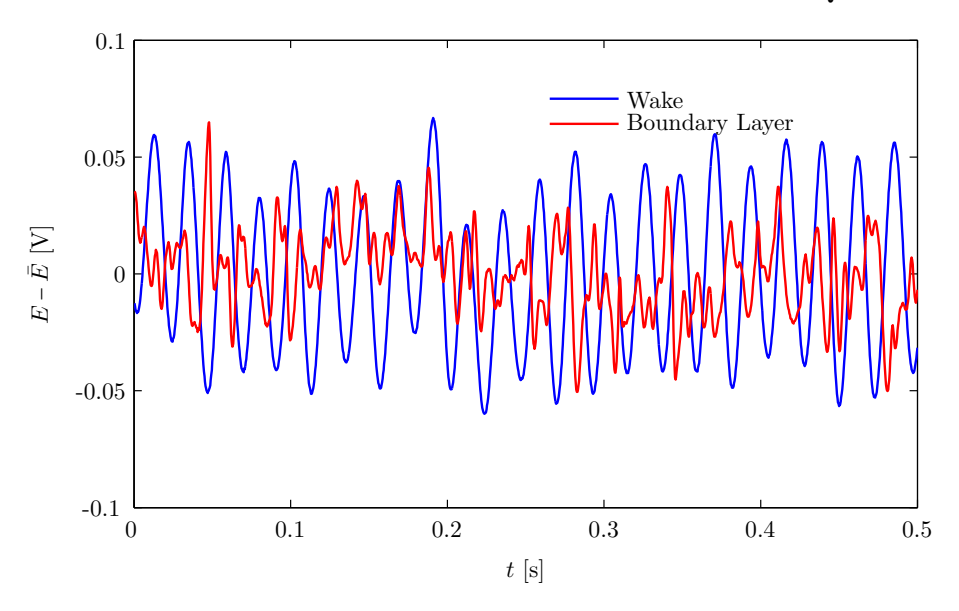


FIGURE 4.6. Sample of the time signal as recorded by the hot-wire in the boundary layer and downstream of the trailing edge, just outside the wake.

section. A number of a-posteriori corrections have to be considered to obtain accurate results. A correction method is described in Paper 1 and will therefore not be repeated here. Examples of a Pitot tube and a Prandtl tube are shown in figure 4.7.

4.3.1. Near-wall boundary layer measurements

When performing near-wall measurements with a Pitot tube, it is common to start the wall normal traverse with the probe touching the wall, or being even slightly bended. As a result, some point close to the wall must be discarded. First, the first derivative of u with respect to y is calculated. All points for which a negative, unphysical, gradient is found are discarded. Then, the second derivative is calculated and all points up to the maximum are discarded as well. This method has been checked extensively and proved to be the best objective method to discard points. An example of a boundary layer measurement and the points that are discarded is shown in figure 4.8. This example is measured in combination with a Furness FC0510 (0-200/2000 Pa, 0.25% FSD) pressure transducer.

The reference static pressure in the boundary layer can be obtained from e.g. a Prandtl probe located in the free stream. It follows from the boundary layer approximation that the static pressure is constant throughout the boundary layer.





FIGURE 4.7. Left: Near wall boundary layer measurement with a Pitot tube. Right: Parallel mounted hot-wire probe (Left) and Prandtl tube (Right) at the extremity of a 1D traverse.

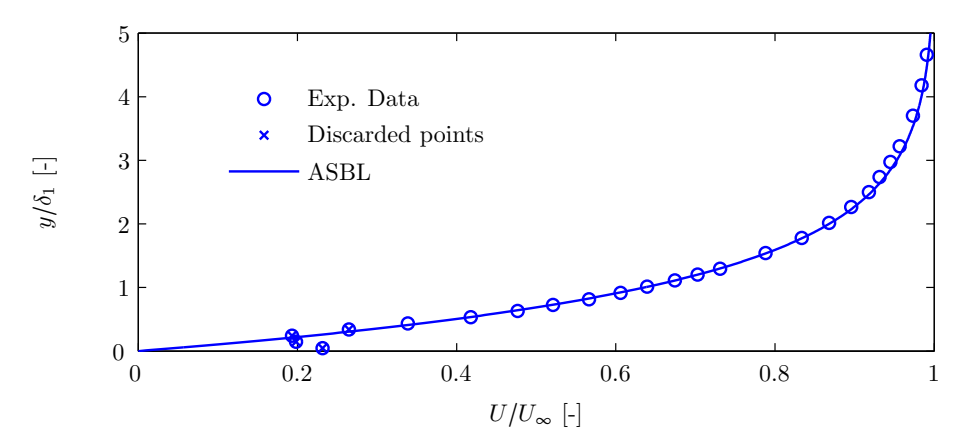


FIGURE 4.8. Boundary layer measurements with a Pitot tube ($U_{\infty}=2.5$ m/s, $V_0/U_{\infty}=0.0057$).

4.3.2. Near-wake pressure measurements

In the far wake, x/h > 30 (Antonia & Rajagopalan 1990), the thin shear layer approximation is valid. Similar to the boundary layer equivalent, the static pressure is constant in the cross stream direction. However, in the near wake this approximation does not hold which means that the static pressure must be measured locally. Therefore a Prandtl tube is used in the near wake.

The design of a static-pressure tube is not straight-forward. In particular the location of the static pressure holes is essential for an accurate pressure measurement (Tropea *et al.* 2007). At the tip of the probe the flow will accelerate. As a result the static pressure will be overestimated up to four diameters downstream. The support or stem downstream of the pressure holes, on the

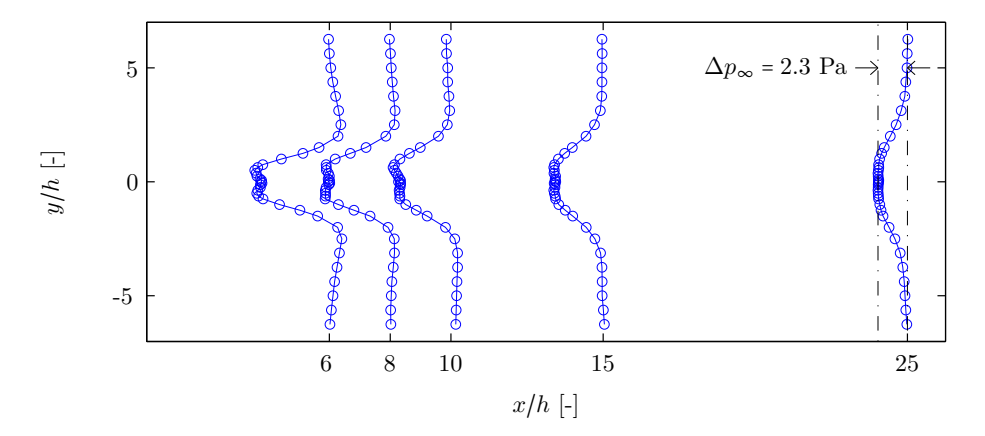


FIGURE 4.9. A relative comparison of the static pressure p_{∞} evolution in the streamwise direction ($U_{\infty} = 10 \text{ m/s}$)

other hand, causes the local static pressure to increase due to the flow deceleration, which extends over twenty probe diameters upstream. Some Prandtl tubes are designed in such a way, L-shaped, that the influence of the tip and support cancel each other out. In the present study, a straight Prandtl tube is used. The static pressure holes are located far enough downstream of the tip and far enough upstream of the traverse stem to avoid influence thereof.

In figure 4.9 the evolution of the static pressure in the streamwise direction is shown, measured with a ScaniValve 16 channel Digitial Sensor Array (2500 Pa, 0.2% FSD) pressure transducer. It is clear that the static pressure recovers, but that it has not fully recovered at x = 25h. The static pressure deficit Δp_{∞} constitutes 23% of the dynamic pressure at x = 6h, which is reduced to 11% at x = 25h. Hence, the use of a Prandtl tube is not redundant.

4.4. Particle Image Velocimetry

Hot-wire anemometry and pressure measurement techniques are not suitable to be used in the recirculation region of a bluff body due to reversed flow direction and strong three dimensionality of the flow. A more appropriate method to use in this type of flow is Particle Image Velocimetry. PIV is non-intrusive and is able to capture the instantaneous flow structure, which can comprise two or three velocity components.

PIV is based on the measurement of the displacement of tracer particles during a short time interval. The tracer particles, e.g. smoke for the application in a wind tunnel, makes the optically transparent fluid visible. Two sheets of particles are illuminated succesively and recorded with a (high-speed) camera. The two images are divided into interrogation areas for which the velocity vector is computed by means of cross correlation. A general description of PIV

can be found in e.g. Raffel $et\ al.\ (2007);$ Adrian & Westerweel (2011). In the remainder of this section, considerations made for accurate measurements will be discussed.

All measurements presented in this thesis were carried out with a Dantec Dynamics PIV system, composed of a Litron DualPower 50–200 (50 mJ, 200 Hz) laser and two SpeedSense M120 cameras (12 bit), which have a sensor resolution of 1920×1200 pixels. The laser power is sufficient to obtain a 25×25 cm² field of view in a gaseous flow seeded with aerosol droplets. The maximum sampling frequency of 200 image pairs per second means the shedding frequency for most flow cases studied in the present work could be resolved. Furthermore, the maximum capacity of the camera of 1825 image pairs in a single recording was sufficient to have converged mean and higher order statistics in a single run.

A Dantec Dynamics Seeding generator was used to generate seeding particles. The atomizer was used to acquire the desired particle density concentration prior to measurements and switched off during the measurements. An oily liquid called Di-ethyl-hexyl-sebacate (DEHS, $\rho_p = 912 \text{ kg/m}^3$) was used as a working fluid, because of the good optical characteristics and a minimum amount of residue. Nonetheless, the perforated surfaces of the body had to be cleaned often to retain its porosity. The particle size is estimated to be in the order of 1 µm based on the atomizer specifications and the reported particle size for DEHS in particular by Raffel $et\ al.\ (2007)$.

The ability of a particle to follow the fluid strongly depends on the particle size in case the particle density is much larger than the fluid it is suspended in, which is typically the case for windtunnel applications. The behavior of a particle in an accelerating flow is often quantified in terms of the relaxation time or the Stokes number. The relaxation time originates from the step response which is exponential for spherical particles at very low Reynolds numbers, i.e. Stokes flow, and is given by Raffel *et al.* (2007):

$$\tau_s = d_p^2 \frac{\rho_p}{18\mu} \ , \tag{4.55}$$

where μ is the dynamic viscosity of the fluid. For DEHS, we find $\tau_s \approx 0.01$ ms and the Stokes number, defined as the ratio between the particle relaxation time and the characteristic time scale of the flow:

$$Stk = \frac{\tau_s U_{\infty}}{h} , \qquad (4.56)$$

where U_{∞} is the free stream velocity and h is the body thickness, is $Stk \ll 0.1$. We conclude that the timescale we wish to resolve is much larger than the relaxation time of the particle and hence, the particles will follow the fluid adequately.

Another important property of the seeding particles is the ability to scatter light, which depends on the refractive index of the working fluid n_p relative to

the refractive index of the surrounding gas n_f . For DEHS and typical other fluids in air, $n_p/n_f \approx 1.5$, the scattering is very efficient and therefore the particles can be small. It is beyond the scope of this thesis to give a full description of the imaging of small particles, see e.g. Goodman (2005). It suffices to mention that the f-number, the magnification and the wavelength affect the size of particle image obtained. These parameters do also effect the depth of field, which is the range of depths where the particles are well focused. It is important that the depth of field is larger than the light sheet thickness to make sure that all particles are well focused. The particle image size must be larger than the pixel size in order to avoid peak locking.

A raw PIV image consist of gray scale values representing the light intensity recorded by each pixel of the camera. The raw image contains particle images and superimposed reflections of the body surface. To remove reflections, which are invariant in time, the ensemble average is subtracted. To compute the velocity field, the images are subdivided into interrogation areas, where the largest window size is based on the particle displacement. A generally accepted rule-of-thumb estimation, sometimes referred to as the 'one-quarter' rule, is that the in-plane and out-of-plane are equal or smaller than 25% of the interrogation window.

The average integer displacement for each interrogation window is given by the cross-correlation peak with respect to the origin. The cross-correlation is FFT-based and a sub-pixel resolution can be obtained if the correlation peaks covers more than a single pixel. The most common PIV algorithms employ a multi-pass scheme, whereby the interrogation area is progressively reduced from the largest to the final window size and the intermediate results are used to pre-shift the two images relative to each other. An improved result can be obtained if an adaptive PIV algorithm is used instead (Scarano & Riethmuller 2000). The adaptive PIV method iteratively optimizes the size and shape of each interrogation area to adapt to local flow gradients and is therefore desired for the complex flow behind a bluff body.

Once all interrogation areas are processed, spurious vectors called outliers can be observed. To find outliers, a universal outlier detection scheme (Westerweel & Scarano 2005) is used, which compares each vectors with the the normalized median of surrounding vectors. Vectors identified as outliers can be replaced at intermediate steps and after the final iteration.

4.5. Sorting PIV images

Ensembles of PIV images obtained in a periodically varying flow is typically randomly organized with respect to phase. To recover the phase information afterwards, an external phase indicator can be used to record simultaneously a time-resolved measurement of a quantity subject to the same periodic variation. A hot-wire recording obtained in the same plane as the PIV snapshots

was obtained for some cases. When hot-wire data was not available, a well established method to obtain the phase averaged properties in the near wake of a bluff body, using only the PIV ensemble, is proper orthogonal decomposition (POD).

In order to elaborate on the POD method, the velocity field $\bar{U}(\vec{x},t)$ must be decomposed into a time-independent component $\bar{U}(\vec{x})$ and a fluctuating component $\bar{u}(x,t)$:

$$\vec{U}(\vec{x},t) = \bar{U}(\vec{x}) + \vec{u}(\vec{x},t) , \qquad (4.57)$$

In case of a periodic flow, like the wake behind a bluff body subject to vortex shedding, the fluctuating component can be written as the sum of a (quasi)-periodic component \tilde{U} and a random fluctuating component \vec{u}' :

$$\vec{u}(\vec{x},t) = \tilde{U} + \vec{u}' \ . \tag{4.58}$$

The POD method decomposes the fluctuating component into a sum of modes $\vec{\phi}_n(\vec{x})$ multiplied with the mode coefficient $a_n(t)$:

$$\vec{u}(\vec{x},t) = \sum_{n=1}^{N} a_n(t) \vec{\phi}_n(\vec{x}) , \qquad (4.59)$$

with N the number of snapshots. To implement the POD method, a scheme for snapshots realignment described by Sirovich (1987) and an implementation of that method similar to that reported by Rehimi $et\ al.\ (2008)$ and Brevis & García-Villalba (2011), is used. The temporal correlation matrix C is introduced first, which is defined as:

$$C = [C_{i,j}] = \int_{D} \vec{u}(x, y, t_i) \cdot \vec{u}(x, y, t_j) dx dy , \qquad (4.60)$$

where D is the spatial domain (Rehimi *et al.* 2008). The eigenvalue problem is than given by:

$$C\vec{A}_n = \lambda_n \vec{A}_n \tag{4.61}$$

where A_n is the *n*th eigenvector corresponding to the *n*th eigenvalue λ_n and the eigenmodes are given by: Brevis & García-Villalba (2011):

$$\vec{\phi}_n(\vec{x}) = \sum_{i=1}^N A_n(t_i) \cdot \vec{u}(x, y, t_j) . \tag{4.62}$$

The eigenvalue λ_n represents the contribution of the corresponding POD mode to the total fluctuating energy. In case of the flow downstream of a bluff body the first two, most energetic, modes are associated with the shedding of vortices (Perrin *et al.* 2007). Van Oudheusden *et al.* (2005) showed that the POD coefficients belonging to these first two modes can be used to determine the phase angle of each snapshot. That is, the phase φ of a snap shot is given by (Ben Chiekh *et al.* 2004; Van Oudheusden *et al.* 2005; Perrin *et al.* 2007):

$$\phi(t) = \arctan\left(\frac{A_2(t)/r(t)}{A_1(t)/r(t)}\right) \quad \text{with, } r(t) = \sqrt{A_1(t)^2 + A_2(t)^2}$$
 (4.63)

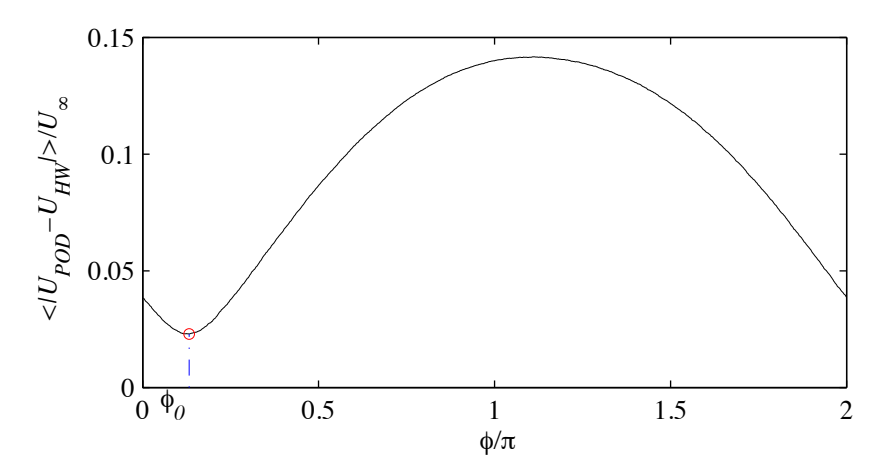


FIGURE 4.10. U_{POD} and U_{HW} represent the streamwise velocity component of the phase-averaged velocity field. The figure shows the discrepancy between the methods when subject to different phase shifts ϕ . The optimum phase shift ϕ_0 is indicated with a red circle.

To validate the phase average obtained by the POD method the results are compared to the phase average based on the phase information from a hot-wire probe. Here, it should be noticed that POD provides only the relative phase. To compare the two different phase sorting methods, the absolute phase shift must be determined. To do so, the spacial average of the phase-averaged velocity field is compared for a phase shift $\phi = 0: 2\pi/1000: 2\pi$, see figure 4.10. For $\phi_0 \approx (2/15)\pi$ the best correlation is found, for which the 'error' is less then 3%.

To examine the methods we go back to the basis of the POD snapshot method. The phase is determined based on the position of the POD coefficients of respectively the first and second mode (a_1,a_2) in the scatter plot. In figure 4.11 this scatter plot is shown, where the pair of POD coefficients corresponding to each snapshot is colored according to the correlation between the contents of the phase bins based on the hot-wire and POD methods. That is, if a snapshot is in the same phase bin for both methods, it is colored green. The color red indicates that the snapshot is found in a neighboring bin and all other points are black. 23% of the snapshots is placed in the same phase bin, independent of the method. If snapshots are aligned by means of the POD snapshot method, and a snapshot in any of the phase bins is considered, 57% will be placed in the same phase bin, or in one of the neighboring phase bins, if instead the hot-wire was used.

Figure 4.12 shows where the snapshots of a single phase bin, realigned by means of the hot-wire, are found in the POD coefficient scatter plot. All

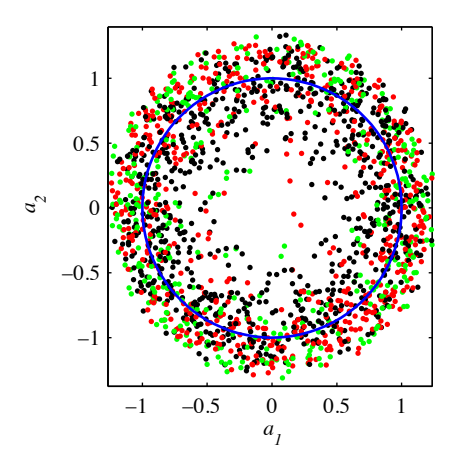


FIGURE 4.11. A scatter plot of the POD coefficient of the first two modes. Points corresponding to snapshots that were placed in the same phase bin for both hot-wire and POD are colored green. Points that were placed in a neighboring bin are depicted in red.

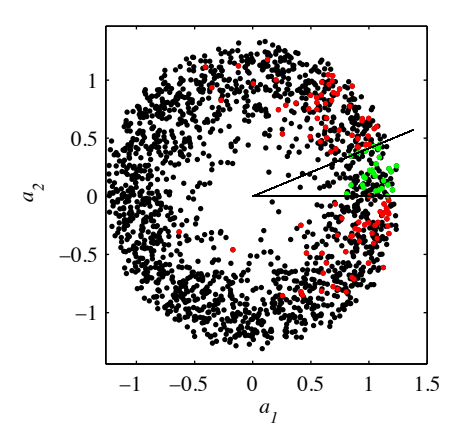


FIGURE 4.12. A scatterplot of POD coefficients is shown. The snapshots of a single phase bin, based on the hot-wire data, are marked with a color other than black. Those snapshots placed in the same bin are colored green and the others red.

snapshots in the considered phase bin are colored red or green. The green symbols mark snapshots that have been assigned the same phase bin. The edges of the phase bin are delineated with black lines. From this plot we could obtain the number of bins that would assure the bin edges are sufficiently far apart to place a satisfactory amount of snapshots in each bin.

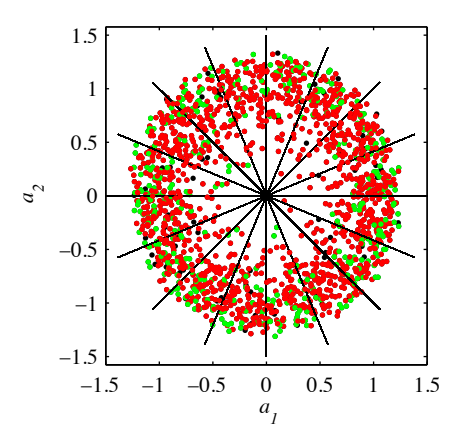


FIGURE 4.13. A scatterplot of POD coefficients where snapshots placed in the same phase bin, independent of the method used to realign, are marked in green. The color red is used otherwise, whereas black indicates points excluded based on the hot-wire signal.

The analysis is extended from a typical phase bin, to all phase bins, see figure 4.13. Snapshots for which no clear phase could be determined with the hot-wire are left black. Snapshots that were assigned to the same phase bin are again green and all the other snapshots result in a red marker. The idea is that this could reveal if a threshold with respect to the radius $r_i = \sqrt{a_1^2(i) + a_2^2(i)}$ could be formulated to exclude snapshots if one uses the POD snapshot method. No obvious correlation between the radius and the correspondence between the methods is shown.

4.6. Vortex detection

The two-dimensional velocity vector fields obtained by PIV in the wake of a bluff body can be used to analyze the effect of suction on the vortex street. In this section the method by which the vortices are detected and characterized will be discussed. The algorithm is based on a vortex detection program described by Fallenius $et\ al.\ (2014)$.

The vortices shed behind a bluff body are typically strong, that is, the vorticity field:

$$\omega_z = \frac{\partial U}{\partial y} - \frac{\partial V}{\partial x} \tag{4.64}$$

reveals roughly the location of the vortices. However, using the maximum vorticity to determine the position of the vortex core might lead to a high uncertainty (Kim *et al.* 2006), because shearing motion gives a high vorticity as well (Adrian *et al.* 2000). Several alternative methods to discern vortices

are based on the velocity gradient tensor $\nabla \vec{u}$ (Jeong & Hussain 1995), which in two-dimensional form is given by:

$$\vec{\nabla}\vec{u} = \begin{vmatrix} \frac{\partial u}{\partial x} & \frac{\partial u}{\partial y} \\ \frac{\partial v}{\partial x} & \frac{\partial v}{\partial y} \end{vmatrix} . \tag{4.65}$$

The eigenvalues of the velocity gradient tensor and the invariants of the corresponding characteristic equation define the flow topology, as described by Chong et al. (1990). In the two-dimensional case, the velocity gradient tensor will either have two real eigenvalues λ_r or a pair of complex conjugate eigenvalues λ_c . Vortices, for which fluid parcels must orbit in a roughly circular path, are identified by regions where the imaginary part of the λ_c is positive: $\lambda_{c,i} > 0$ (Adrian et al. 2000).

Figure 4.14 shows a typical example of the distribution of $\lambda_{c,i}$ in the wake of a bluff body. To smooth out small scale variations, a uniform filter is applied, which replaces each value by the average value over a 5×5 subdomain. A single vortex is defined as a local patch where the eigenvalue exceeds a given threshold.

The vortex core is defined by either the vortex peak or the vortex centroid. Within the formation region, the vortex peak, here defined as the maximum $\lambda_{c,i}$, gives a better estimate because the vortex contour exhibits strong asymmetry. Beyond the formation region the contour has become roughly circular, and an integrated value improves the estimate. The centre of the centroid is found by fitting a circle, with a surface equal to half the area spanned by the contour, to maximize the integral value. A similar hybrid method is described by Kim *et al.* (2006).

Once the vortex is defined, the circulation can be calculated. The circulation γ around a closed contour C is defined as the line integral of the tangential velocity:

$$\gamma \equiv \oint_C \vec{u} \cdot d\vec{r} \ . \tag{4.66}$$

Here, the integral is carried out over a circular path with an equivalent radius as to enclose the same surface area as the vortex. The center of the subsidiary area corresponds to the vortex core.

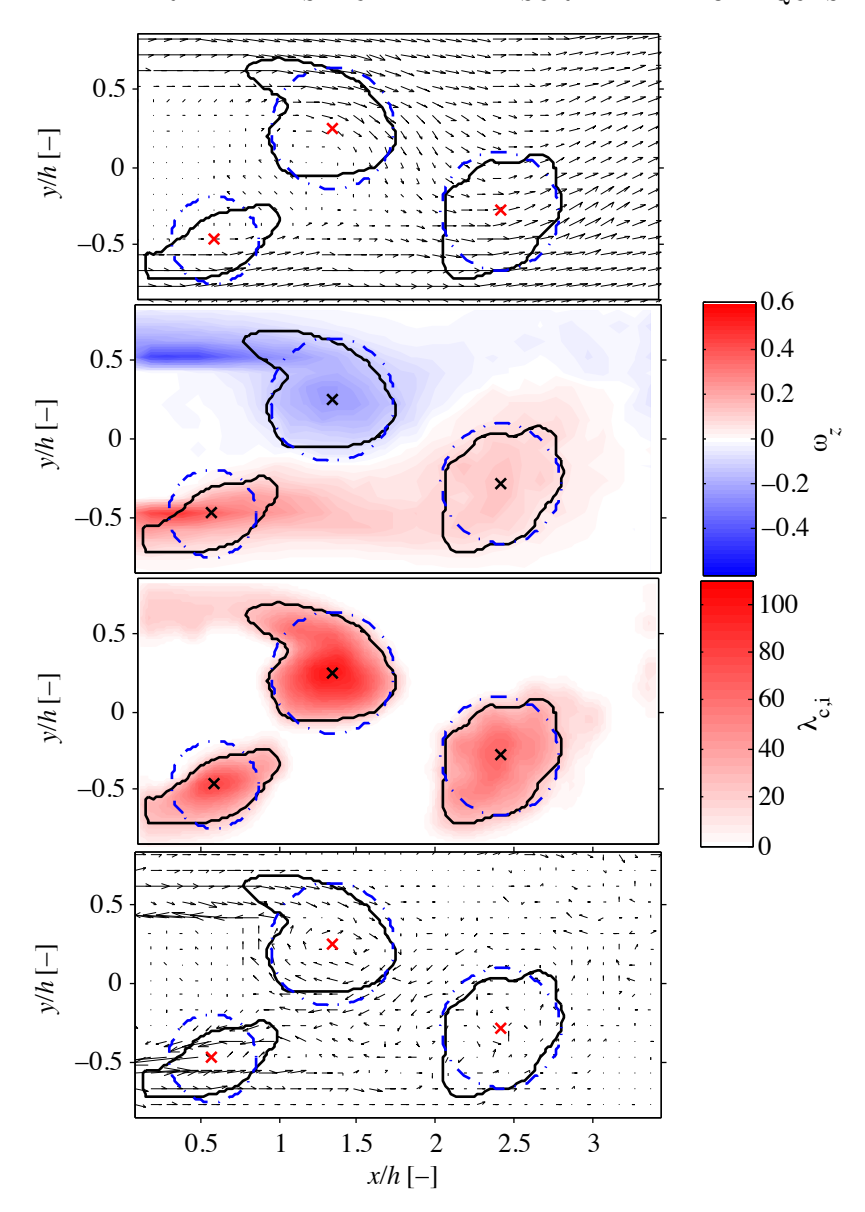


FIGURE 4.14. A typical example of the phase-averaged flow topology, visualized by: (a) the velocity vectors, (b) the vorticity ω_z , (c) the complex part of the eigenvector $\lambda_{c,i}$, and (d) the high-pass filtered field. The vortex contour is delimited with a black line, the equivalent circular area is surrounded by a blue dashed line and the vortex center is marked with a black or red cross $(Re_h = 6.7 \times 10^3, \Gamma = 0)$

CHAPTER 5

Summary of results

In this chapter, a selection of results from the papers appended in the second part of this thesis will be presented to illustrate the scope of the research conducted. Reference will be made to the corresponding paper, where a detailed discussion and more results can be found.

5.1. Boundary layer properties

The laminar boundary layer subject to wall suction is discussed in paper 2, and the turbulent boundary layer subject to wall suction is included in paper 3. Measurements were carried out in the range $Re_h = 2.9 \times 10^3 - 5.5 \times 10^4$, as shown in table 1. The flow cases are divided into laminar (L) and turbulent (T), based on the state of the boundary layer at the trailing edge for the neutral suction case ($\Gamma = 0$). For $Re_h \le 6.7 \times 10^3$, the boundary layer remained laminar up to the trailing edge, whereas for $Re_h \ge 8.0 \times 10^3$ the boundary layer was observed to be transitional. To avoid transient boundary layers for the neutral suction case, a tripping tape was placed at the leading edge for the turbulent cases

The development of the displacement thickness $\delta_{1,x}$ in the flow direction, with and without wall suction, is shown in figure 5.1. $\delta_{1,x}$ is normalized by the displacement thickness at $x_0=0.3$ m. It is from this location and onward that wall suction is applied. The theoretical value of the ASBL is subtracted from $\delta_{1,x}$ and the reference value δ_{1,x_0} , such that the normalized displacement thickness asymptotes to zero when the ASBL solution is approached. Without wall suction, the experimental data initially coincides with the theoretical profile for the Falkner-Skan boundary layer, see equation 3.23. For $Re_x > 3.5 \times 10^5$ the experimental data falls below the theoretical curve, which is due to the upcoming trailing edge. When wall suction is applied, $\Gamma=5.6$, the displacement thickness decreases and approaches zero, and hence, the ASBL solution is obtained. The experimental data is in good agreement with the theoretical relation by Rheinboldt (1955), see equation 3.33. Again, the displacement thickness starts to deviated from the theoretical relation when approaching the trailing edge of the body.

The effect of suction on laminar boundary layers is shown in figure 5.2. The mean velocity profiles are measured 1h upstream of the trailing edge by

Table 1. An overview of the studied flow cases. The state of the boundary layer for neutral suction ($\Gamma = 0$) is either laminar (L) or turbulent (T). The symbols shown here will be used consistently in figures, with the face color grayscale as an indicator of the wall-normal velocity V_0 , black being the neutral suction case ($V_0 = 0$).

Symb.	BL State	U_{∞} [m/s]	Re_h [-]	Re_x [-]	Γ Max.
0	${ m L}$	1.0	2.9×10^{3}	1.6×10^{5}	28.4
\triangleleft	${ m L}$	1.5	4.1×10^3	2.3×10^5	21.4
	${ m L}$	2.0	5.3×10^3	3.0×10^5	16.1
Δ	L	2.5	6.7×10^3	3.8×10^5	13.6
\triangleright	${ m T}$	5.0	1.4×10^{4}	7.7×10^{5}	6.6
$\stackrel{\wedge}{\Longrightarrow}$	${ m T}$	10.0	2.7×10^{4}	1.6×10^{6}	3.2
∇	${ m T}$	15.0	4.1×10^4	2.3×10^6	2.1
苁	${ m T}$	20.0	5.5×10^{4}	3.0×10^{6}	1.6

means of hot-wire anemometry. This position is a trade off between having a measure of the boundary layer representative of the inlet conditions of the wake and being able to make accurate measurements with a hot-wire. As was shown in figure 5.1, the boundary layer thickness is already reduced due to the upcoming trailing edge at this location.

To emphasize that a relatively small suction coefficient has a significant impact on the boundary-layer thickness, the unscaled mean velocity profiles for $Re_h = 6.7 \times 10^3$ are shown in figure 5.2(a). It is observed that an increase of the suction coefficient leads to a decrease of the boundary layer thickness and an increase of the wall shear stress. The displacement thickness and the momentum thickness, normalized with the theoretical ASBL value for the displacement thickness given by equation 3.27, are shown in figure 5.2(b). For $\Gamma \approx 4$ an overshoot is observed, which is explained by the ordinary boundary layer without suction being thicker. For $\Gamma > 9$ the ASBL is reached, which can be concluded from the fact that the normalized displacement and momentum thickness have reached a constant value of 1.0 and 0.5, respectively.

In figure 5.3(a) the mean velocity profiles for turbulent boundary layers subject to suction coefficients in the range $\Gamma = 0.0 - 3.2$ are shown for $Re_h = 2.7 \times 10^4$ in inner scaling. The wall position and the friction velocity were obtained from the experimental data in a least-square fit algorithm based on equation 3.49. For a high level of wall suction the turbulent boundary layer

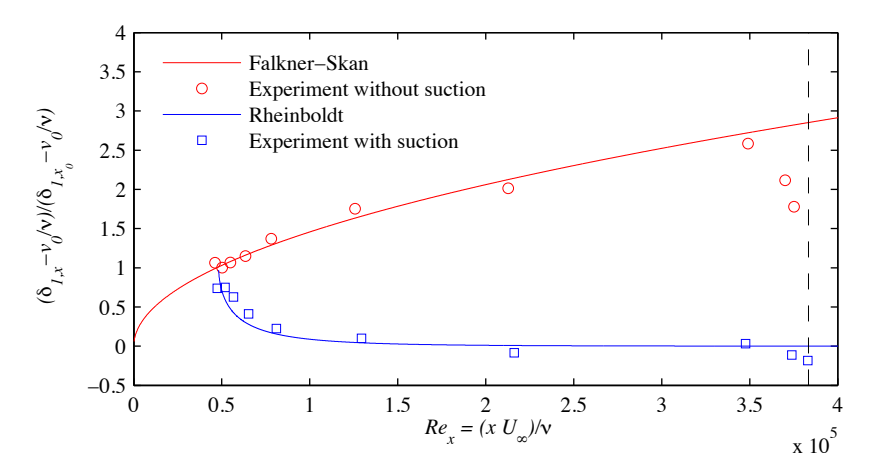


FIGURE 5.1. The development of the boundary layer thickness $\delta_{1,x}$ in the streamwise direction x over the perforated surface plotted as function of the Reynolds number Re_x . The case without suction ($\Gamma=0$) is compared to the case with wall suction ($\Gamma=5.8$) for $Re_h=6.7\times 10^3$. The Reynolds number corresponding to the trailing edge is marked with a dashed line.

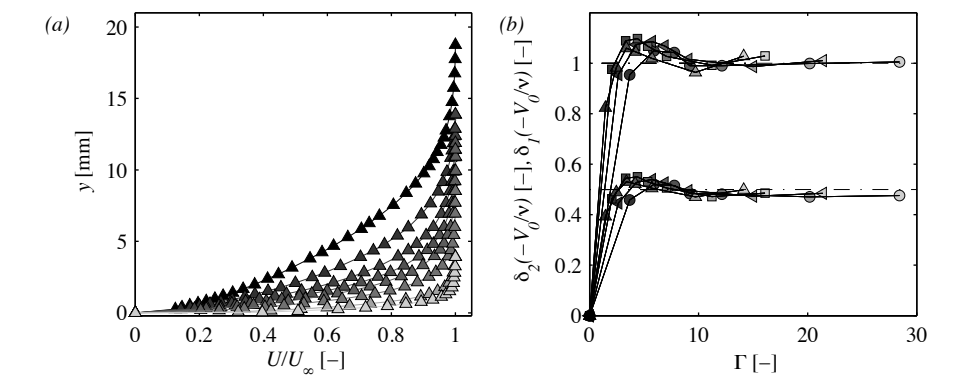


FIGURE 5.2. The effect of wall suction on a laminar boundary layer illustrated by: (a) the unscaled mean velocity profiles for suction coefficients in the range $\Gamma = 0.0 - 13.6$ for $Re_h = 6.7 \times 10^3$, and (b) the displacement thickness δ_1 and the momentum thickness δ_2 normalized by the theoretical value for the ASBL plotted as function of the suction coefficient Γ . Symbols as defined in table 1

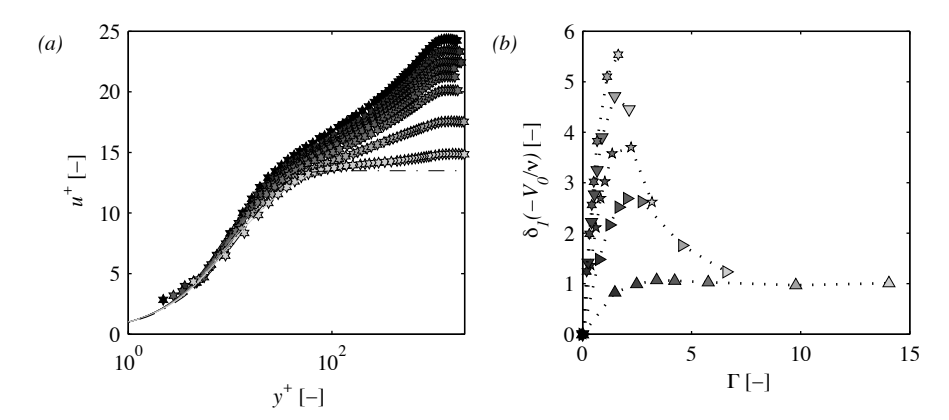
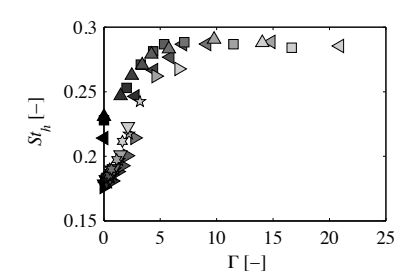


FIGURE 5.3. The effect of wall suction on a turbulent boundary layer illustrated by: (a) the mean velocity profiles in inner scaling for suction coefficients in the range $\Gamma = 0.0 - 3.2$ for $Re_h = 2.7 \times 10^4$, where the dash-dotted line represent the theoretical ASBL. And (b) the displacement thickness δ_1 and the momentum thickness δ_2 normalized by the theoretical value for the ASBL plotted as function of the suction coefficient Γ . Symbols as defined in table 1

approaches the laminar ASBL (dash-dotted line), which is an indication that the boundary layer relaminarizes. This is illustrated in figure 5.3(b) as well, which shows the displacement thickness normalized by the theoretical value for the ASBL for turbulent boundary layers subject to suction. For comparison, a laminar case ($Re_h = 6.7 \times 10^3$, \triangle) is included as well. The normalized displacement thickness increases as the direct effect of V_0 is stronger than the indirect effect of δ_1 until they compensate for each other and the curve reaches a maximum. The maximum seems to mark the onset of relaminarization whereafter the indirect δ_1 is dominating. Similar values of Γ for the onset of relaminarization have been found numerically (Schlatter & Örlü 2011; Khapko 2014).

5.2. Wake characteristics

For the range of Re_h and Γ investigated, a significant change of the wake characteristics was obtained by a modification of the boundary layer properties. This is illustrated in figure 5.4, which shows the Strouhal number and the base pressure coefficient as function of the suction coefficient. For $\Gamma > 9$, the Strouhal number and the base pressure coefficient approach values of $St \approx 0.28$ and $C_{p,b} \approx -0.35$, respectively, which coincides with Γ values for which the ASBL was obtained. This is a first indication that the shape factor, which is constant for the ASBL, should be considered to find a relation between the wake characteristics and the wake inlet conditions.



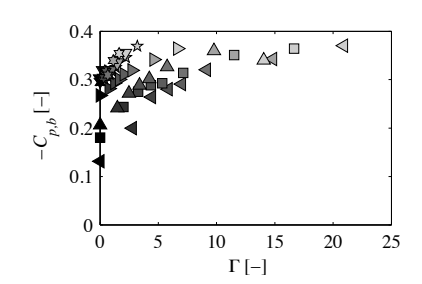


FIGURE 5.4. The Strouhal number St_h and the base pressure coefficient $C_{p,b}$ are plotted as function of the suction coefficient Γ in (a) and (b), respectively. Symbols as defined in table 1

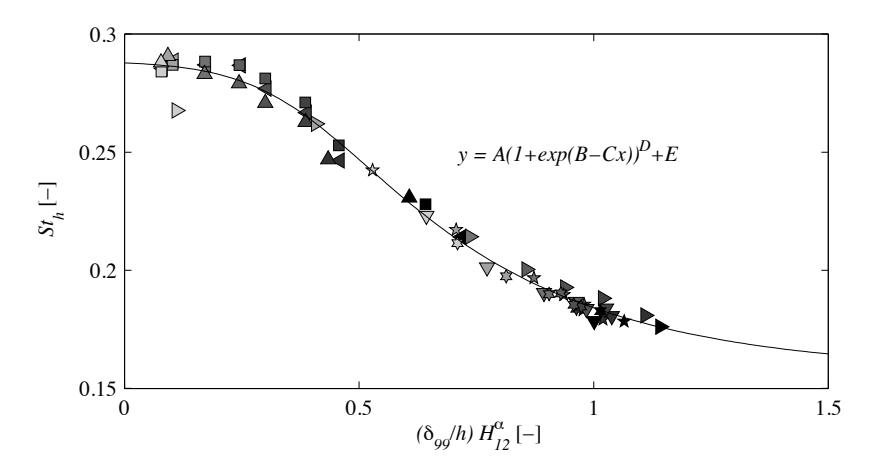


FIGURE 5.5. The Strouhal number St_h as function of the normalized boundary layer thickness δ_{99}/h , multiplied with the shape factor H_{12} weighted with a coefficient $\alpha=0.45$, is shown. A Richards' equation is fitted in a least-square algorithm to find $A=0.13,\ B=-3.6,\ C=-9,5,\ D=-0.27$ and E=0.16. Symbols are defined in table 1.

Various scalings for the relation between the boundary layer properties and the wake characteristics have been reported in paper 2, paper 3, and paper 5. It is recognized that the most obvious choice is a scaling based on the displacement thickness, since the physical meaning is inherently related to the bluff body shape. However, the displacement thickness does not properly represent the wall-normal velocity gradient, which is distinctively different for laminar and turbulent boundary layers and is thought to play an important role in the formation of vortices. Naturally, the shape factor would be included to correct

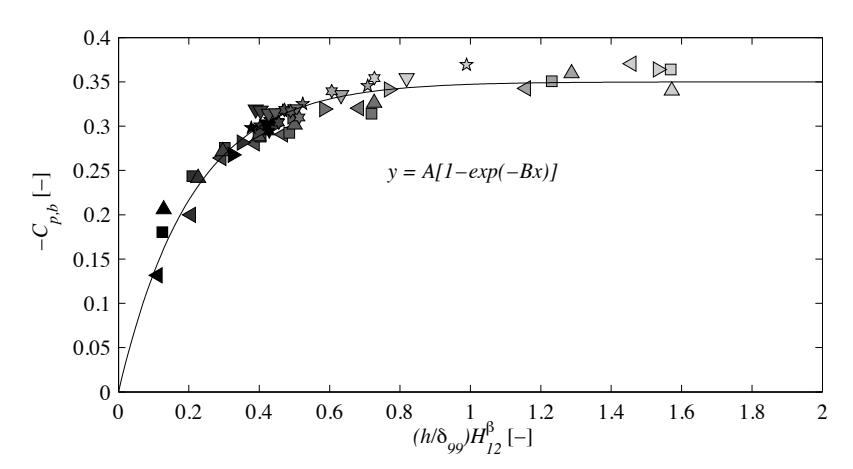


FIGURE 5.6. The base pressure coefficient $C_{p,b}$ as function of the reciprocal of the normalized boundary layer thickness δ_{99}/h , multiplied with the shape factor H_{12} , weighted with a coefficient $\beta = -3.4$, is shown. A least-square fit algorithm was employed to fit an exponential equation with coefficient A = 0.35, B = 4.8. Symbols are defined in table 1.

for this, but it annihilates partially the effect of the inclusion of the displacement thickness. Therefore, an empirical relation is sough after based on the boundary layer thickness δ_{99} , in combination with the shape factor H_{12} .

A least-square fit algorithm is used to obtain an expression in terms of the normalized boundary layer thickness δ_{99}/h scaled with the weighted shape factor H_{12}^{α} . The exponent $\alpha=0.45$, included as a fitting parameter, weakens the strength of the scaling parameter H_{12} . All the data is found to collapse on a single curve best represented by a Richards equation as shown in figure 5.5. When the boundary layer thickness becomes negligible compared to the base height, i.e. $\delta_{99}/h \rightarrow 0$, the Strouhal number approached $St \approx 0.29$. On the other hand, when the boundary layer is large compared to the base height, the Strouhal number exponentially decays towards $St \approx 0.16$.

A similar relation based on the boundary layer thickness, and including the weighted shape factor H_{12}^{β} was looked after for the base pressure coefficient. The result is shown in figure 5.6. A least-square fit algorithm is employed to find the $A=0.25,\ B=4.8$ and $\beta=-3.4$. The empirical relation takes into account that the base pressure should be equal to the free-stream pressure if the body height is negligible, When the body height is much larger than the boundary layer thickness, i.e. $h/\delta_{99} \to \infty$, the base pressure coefficient asymptotes towards $C_{p,b}=-0.35$.

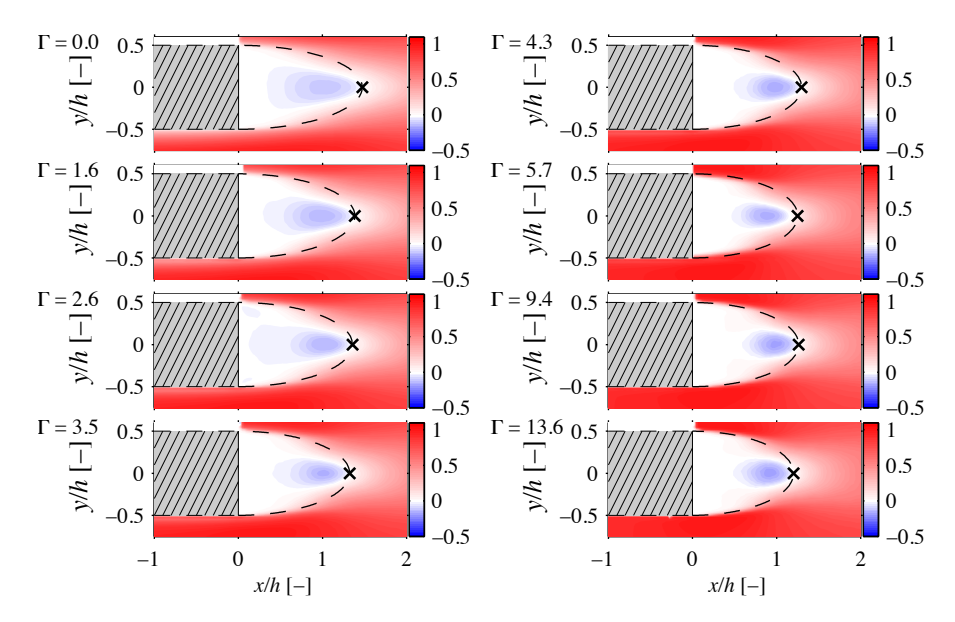


FIGURE 5.7. The mean velocity field $\bar{u}(\vec{x})$ for $Re_h = 6.7 \times 10^3$ visualized by contours of the streamwise velocity component. The confluence point is marked by a cross (×) and the boundary of the formation region is indicated by a dashed-line.

5.3. Near wake topology

A velocity field $\vec{U}(\vec{x},t)$ behind a bluff body can often be decomposed into a time-independent component $\bar{u}(\vec{x})$, a periodic component $\tilde{u}(\vec{x},t)$ and a fluctuating component $u'(\vec{x},t)$:

$$\vec{U}(\vec{x},t) = \bar{u}(\vec{x}) + \tilde{u}(\vec{x},t) + u'(\vec{x},t) . \tag{5.67}$$

The time-independent component will be considered first, which is the mean velocity field if one considers a complete ensemble of PIV images. The mean velocity field reveals the formation region, or recirculation region, which is enclosed by the streamlines separating from the body trailing edge. A modification of the boundary layer can lead to a significant change of the formation region, which is illustrated in figure 5.7, which shows the mean velocity field for different Γ at $Re_h = 6.7 \times 10^3$. The end of the formation region is marked by the confluence point, here defined as the saddle point where both the wall-normal as well as the streamwise velocity component are equal to zero. The formation region contour is approximated by a semi-ellipse, with the semi-minor axis equal to the body thickness h and the semi-major axis closing the contour at the confluence point. It is observed that a larger suction coefficient, and hence, a thinner boundary layer, leads to a shorter formation region.

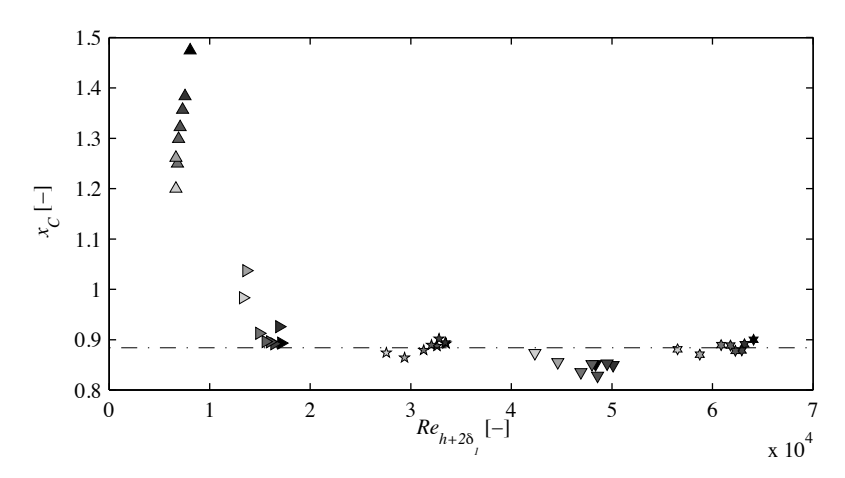


FIGURE 5.8. The confluence point x_C plotted against the Reynolds number based on the effective plate thickness $Re_{h+2\delta_1}$. Symbols are defined in table 1.

In figure 5.8 the confluence point is shown as function of the effective Reynolds number $Re_{h+2\delta_1}$. In the laminar boundary layer case, $Re_{h+2\delta_1} < 1 \times 10^4$, $x_C = 1.47h$ for $\Gamma = 0$ and reduces by 19% when the suction coefficient is increased to $\Gamma = 13.6$. The reduction of the confluence point is ascribed to a shift in the upstream direction of the point of transition of the initially laminar shear layer to turbulence. In case the boundary layer is turbulent at the point of separation, this shift would not occur, which is consistent with the confluence point $x_C = 0.87h$ on average for those cases. Here, the cases for $Re_h = 1.4 \times 10^4$ ($^{\triangleright}$) subject to the two highest suction coefficient (lightest shades of gray) were excluded because relaminarization is evident.

A complete description of the mean recirculation region, including an analysis of the curvature of streamlines, is presented in paper 4 for the laminar cases and extended to the turbulent regime in paper 5.

5.4. Total, periodic and random velocity component

Subtracting the mean velocity field from the ensemble of instantaneous velocity fields results in the total fluctuations;

$$u = \vec{U}(\vec{x}, t) - \bar{u}(\vec{x}) = \tilde{u}(\vec{x}, t) + u'(\vec{x}, t) . \tag{5.68}$$

In figure 5.9 the corresponding Reynolds shear stresses and Reynolds normal stresses are shown for $Re_h=6.7\times 10^3$, and $\Gamma=0.0-13.6$. Considering the peak values, one can conclude that the Reynolds stresses are larger when suction is applied. For the neutral suction case the maxima of \overline{uv} , \overline{uu} and \overline{uv} are 4.0%, 9.8% and 16.9% of U_∞^2 , respectively, whereas for $\Gamma=13.6$ the maxima are 6.2%, 12.4% and 22.7% of U_∞^2 . A similar trend is found for the turbulent

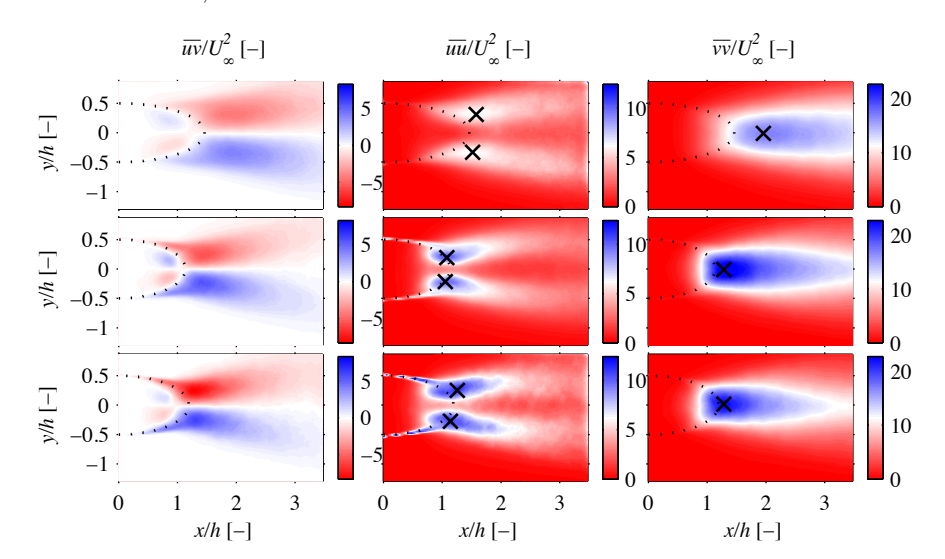


FIGURE 5.9. The Reynolds shear stress (\overline{uv}) and Reynolds normal stress $(\overline{uu}, \overline{vv})$ distributions for three suction coefficients (top: $\Gamma = 0$, middle: $\Gamma = 5.7$, bottom: $\Gamma = 13.6$) at $Re_h = 6.7 \times 10^3$. The recirculation region contour is marked with a dotted line, and the location of maxima for the Reynolds normal stresses are marked with (×)-symbols.

cases at higher Reynolds numbers (not shown). The increase of the velocity gradients within and in close proximity to the recirculation region may explain this increase. The stronger velocity gradient is due to the shortened formation region and the increased curvature of the streamlines in this region, when suction is applied. As a result a similar displacement of a fluid parcel results in a larger velocity fluctuation. A further analysis comprising a balance of the forces acting on the formation region boundary is presented in paper 5.

The total fluctuations can be decomposed into periodic and random fluctuations. The periodic velocity component is characterized by the formation and convection of vortices, and as result, the streamwise and wall-normal velocity component will vary roughly sinusoidally in time. The snapshots of a complete ensemble of PIV images were subdivided into a discrete number of phase bins N_b , based on their phase-angle ϕ in the shedding cycle. The phase-angle ϕ of individual snapshots was found by using an additional hot-wire probe as a phase-indicator for $Re_h = 6.7 \times 10^3$. The POD method presented in section 4.5 was used for the other cases.

The mean of the snapshots in each bin is approximately equal to the phase-average, which provides information on individual vortices. The effect of wall-suction on the vortices formed, i.e. strength and size, is presented in paper 5.

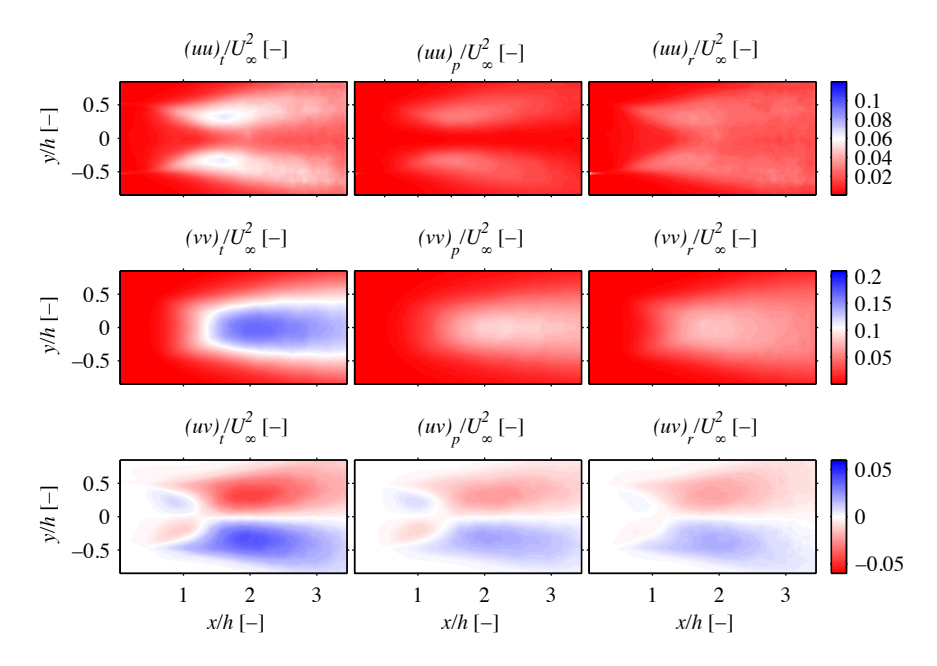


FIGURE 5.10. Contours of Reynolds stresses $[(uu)_t, (vv)_t, (uv)_t]$ and the contributions of the periodic $[(uu)_p, (vv)_p, (uv)_p]$ and random $[(uu)_r, (vv)_r, (uv)_r]$ fluctuations, for $Re_h = 6.7 \times 10^3$ and $\Gamma = 0$.

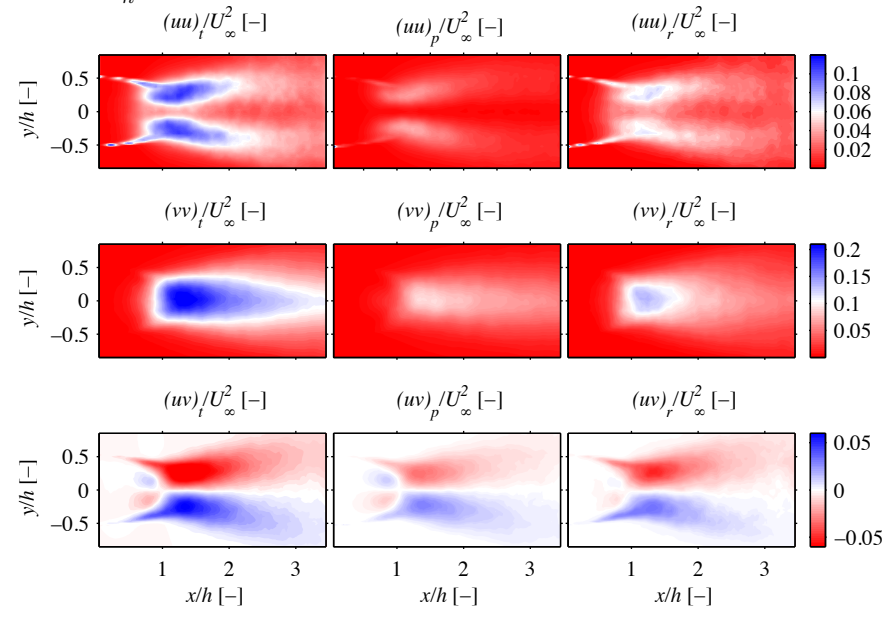


FIGURE 5.11. Contours of Reynolds stresses $[(uu)_t, (vv)_t, (uv)_t]$ and the contributions of the periodic $[(uu)_p, (vv)_p, (uv)_p]$ and random $[(uu)_r, (vv)_r, (uv)_r]$ fluctuations, for $Re_h = 6.7 \times 10^3$ and $\Gamma = 13.6$.

Here, the effect of boundary layer modification on the distribution of the total fluctuating energy over the periodic and random component will be discussed. The phase-average presented here is based on N_b = 128, which corresponds to five snapshots per phase-bin on average.

The contours of the total Reynolds shear stress $(uv)_t$ and the total Reynolds normal stresses $(uu)_t$ and $(vv)_t$, as well as the contributions of the periodic fluctuations $[(**)_p]$ and random fluctuations $[(**)_r]$, are shown in figure 5.10 for $Re_h = 6.7 \times 10^3$ and $\Gamma = 0$. By definition, the sum of the periodic and random component must be equal to the total Reynolds stresses. For the neutral case, with a laminar boundary at the trailing edge, the periodic components $(uu)_p$, $(vv)_p$ and $(uv)_p$ constitute 38%, 49% and 53% of the total Reynolds stresses, respectively. These values are based on the mean value of the domain depicted in figure 5.10.

It was observed before that the total Reynolds stresses increase when suction is applied. The increase is mainly due to an increase of the random fluctuations, which can be concluded from figure 5.11. For $Re_h=6.7\times 10^3$ and $\Gamma=13.6$, $(uu)_p$, $(vv)_p$ and $(uv)_p$ represent 29%, 42% and 42% of the total velocity fluctuations, respectively. A significant contribution of $(uu)_r$ to $(uu)_t$ on the edge of boundary of the mean recirculation is identified, an increase that was previously related to an increase of the force on, and a shortening of, the formation region. A similar shift from the periodic to the random fluctuations is found for Re_h for which the boundary layer is turbulent at the point of separation, as shown in paper 5.

The increase in the Reynolds stresses with wall-suction is due to an increase of the random velocity component. The total Reynolds normal stress in the streamwise direction increases with 25% and 23%, going from no wall suction to $\Gamma_{\rm max}=13.6$ and $\Gamma_{\rm max}=1.6$, for $Re_h=6.7\times 10^3$ and $Re_h=5.5\times 10^4$, respectively. This increase is entirely accounted for by an increase of the random component as the periodic component even slightly decreases. The total Reynolds normal stress and the total Reynolds shear stress remain unchanged with increase in suction, but some energy is shifted from the periodic component to the random component.

To obtain a further understanding of the complex mechanism of vortex formation in the near wake, a splitter plate was introduced. The results of this study are presented in paper 6.

CHAPTER 6

Conclusions

The goal of this thesis is to contribute to the fundamental understanding of the bluff body wake instability and, in particular, the relation between the wake inlet conditions and the wake characteristics. Hot-wire anemometry, pressure measurements and PIV were employed to evaluate a new experimental setup, and to quantify the boundary layer prior to separation, the near wake topology, and the far wake region. For Reynolds numbers in the range $Re_h = 2.9 \times 10^3 - 5.5 \times 10^4$ the following conclusions are drawn:

Experimental validation of the setup

- Boundary layer modification by means of wall suction makes it possible to perform unique parametrical studies.
- The flow over the forebody and in the wake is symmetric and twodimensional, however, for $U_{\infty} \leq 2.5$ m/s the velocity distribution in the wake and the base pressure distributions at the trailing edge show a significant influence from the side walls.

Boundary layers subject to wall suction

- The ASBL is obtained at the trailing edge for $\Gamma > 9$, and Reynolds numbers in the range $Re_h = 2.9 \times 10^3 6.7 \times 10^3$.
- Initially turbulent boundary layers subject to wall suction can relaminarize when the suction coefficient $\Gamma > 3.5$.

Wake characteristics

- A decrease of the displacement thickness leads to a decrease of the base pressure, i.e. the base pressure becomes more negative, in agreement previous observations reported in the literature.
- In the ABSL limit the vortex shedding frequency and the base pressure become $St \approx 0.28$ and $C_{p,b} \approx -0.35$, respectively, except for $Re_h = 2.9 \times 10^3$.
- Empirical relations are formulated for both the vortex shedding frequency and the base pressure based on the normalized boundary layer thickness multiplied by the weighted shape factor.

Near-wake topology

• When the shear layers separating from the surface of the body are laminar, strong evidence was found that the point of transition to turbulence

moves closer to the body under the influence of wall-suction, and as a result, the confluence point was found to move upstream by as much as 19%. For initially turbulent shear layers, the confluence point does not significantly shift under the effect of wall suction for the range of Γ values studied.

- A modification of the boundary layers leads to an increase of the Reynolds normal and shear stresses. The increase in Reynolds normal stress was found to be associated to an increase in random fluctuations, whereas the contribution of the periodic fluctuation component remained unchanged when wall suction was applied.
- The larger velocity gradient due to wall suction leads to an increase
 of the strength and a reduction of the size of the vortices being shed.
 A significant increase in the vortex strength was only observed for the
 laminar cases.
- The curvature of the streamlines enclosing the trailing edge of a rectangular body was shown to be linearly related to the base pressure, but a clear difference between laminar and turbulent separating boundary layers was found.

Splitter plate

- The qualitative effect of a splitter plate on the wake characteristics does not change when the boundary layer is modified, except for the absence of a damping effect on transverse oscillations of the shear layer for attached splitter plates of $L/h \le 0.5$.
- Boundary-layer modification does lead to a decrease of the critical splitter plate length and gap width required to suppress vortex shedding.
- When the splitter plate length is one quarter of the body height the base pressure is reduced by approximately 50% compared to the case without a splitter plate. The location of the splitter plate for which the maximum reduction occurs, shifts downstream when wall suction is applied.
- PIV snapshots confirmed the existence of Bloor-Gerrard vortices when the boundary layer was laminar at the point of separation ($Re_h = 0.7 \times 10^4$). The vortices were shown to coexist with the primary vortex shedding phenomenon for some splitter plate configurations.

Linear stability analysis

- A linear stability analysis based on the measured mean velocity field and Reynolds stresses can predicted the Strouhal number within 3% for the flow cases studied here.
- An experimentally obtained control map is shown to be in good agreement with the results of the numerical sensitivity analysis based on the experimental mean velocity field, considering all limitations of such an experiment.

CHAPTER 7

Papers and authors contributions

Paper 1

A new test section for wind tunnel studies on wake instability and its control. Bengt E. G. Fallenius (BF), Renzo Trip (RT) & Jens H. M. Fransson (JF) Published in *Technical Report*, TRITA-MEK 2014:08 (2014)

This paper is written by BF and RT with feedback from JF. RT wrote the chapter on the experimental validation of the setup and performed the measurements described in this chapter. Parts of this work have been presented at the 9th European Fluid Mechanics Conference 2012, Rome, Italy.

Paper 2

An experimental study on the wake of a rectangular forebody with suction applied over the surfaces.

Renzo Trip (RT) & J. H. M. Fransson (JF).

Published in Proceedings of International Conference on Jets, Wakes and Separated Flows (ICJWSF 2013), 17-21 Sept., Nagoya, Japan, pp. 1042 1–5 (2013)

This conference paper is written by RT with feedback from JF. The experimental data described in the paper are obtained and analyzed by RT with guidance of JF.

Paper 3

An experimental study on the wake behind a rectangular forebody with a laminar and turbulent suction boundary layers.

Renzo Trip (RT) & J. H. M. Fransson (JF).

Published in *Phys. Fluids*, **26** (12), 125105 (2014)

RT planned, performed and analyzed the experiments shown in this paper under supervision of JF. The paper was written by RT with feedback from JF.

Paper 4

An experimental study on the wake behind a rectangular forebody with a laminar and turbulent suction boundary layers.

Renzo Trip (RT) & J. H. M. Fransson (JF).

To appear in Proceedings of International Conference on Jets, Wakes and Separated Flows (ICJWSF 2015), 15-18 June, Stockholm, Sweden (2015)

This conference paper is written by RT with feedback from JF. The experimental data described in the paper are obtained and analyzed by RT with guidance of JF.

Paper 5

On the effect of boundary layer modification on the near wake topology of a rectangular forebody.

Renzo Trip (RT) & J. H. M. Fransson (JF).

RT planned, performed and analyzed the experiments shown in this paper under supervision of JF. The paper was written by RT with feedback from JF.

Paper 6

An experimental study on the combined effect of boundary layer modification and a splitter plate on the wake characteristics.

Renzo Trip (RT) & J. H. M. Fransson (JF).

RT planned, performed and analyzed the experiments shown in this paper under supervision of JF. The paper was written by RT with feedback from JF.

Paper 7

Investigation of passive control of the wake past a thick plate by stability and sensitivity analysis of experimental data.

Simone Camarri (SC), Renzo Trip (RT) & J. H. M. Fransson (JF).

RT planned, performed and analyzed the experiments shown in this paper under supervision of JF. The numerical code to perform the linear stability analysis was written and employed by SC. SC wrote the paper with input form RT and JF.

Parts of the results have been presented by the author:

- 9th Euromech Fluid Mechanics Conference (EFMC-9), 9-13 Sept., Rome, Italy (2012)
- 4th International Conference on Jets, Wakes and Separated Flows (ICJWSF-2013), 17-21 Sept., Nagoya, Japan, (2013)
- 67th Annual Meeting Division of Fluid Dynamics (APS), 23–25 Nov., San Francisco, USA (2014)
- 5th International Conference on Jets, Wakes and Separated Flows (ICJWSF 2015), 15–18 June, Stockholm, Sweden (2015)

CHAPTER 8

Acknowledgements

A PhD project can not be brought to a good end without the guidance, the knowledge, the craftsmanship, the support and the company of others. I would therefore like to express my sincere gratitude to everyone who has contributed to the work presented in this thesis and devote a few lines to those of special importance.

First of all, I would like to thank my supervisor, prof. Jens Fransson, for his trust in me as a future researcher, and for providing me with the knowledge and support required in the process of becoming.

Here, I should also thank my co-supervisor, Dr. Bengt Fallenius, who has not only provided me with a well thought-out experimental setup but also introduced me to experimental techniques and helped me out on numerous occasions solving problems that seemed insurmountable.

And, although our collaboration was limited, I consider the linear stability analysis carried out by my other co-supervisor, associate prof. Simone Camarri, to be a valuable addition to the work presented in this thesis.

Being my roommates and part of the same research group, Dr. Sohrab Sattarzadeh and Marco Ferro deserve a special word of thanks. Often, they were the first ones to turn to when the dynamics of a fluid confused me. And in the privacy of the room, a laugh or a heated discussion were never far away.

Prof. Alessandro Talamelli, Docent Ramis Örlu, Dr. Robert Downs, Dr. Nils Tillmark, Dr. Sissy Kalpakli Vester, and Dr. Antonio Segalini have been most helpful by sharing their broad knowledge and experience in the field of (experimental) fluid mechanics.

The fluid physics laboratory has been a pleasant and inspiring working environment, for which Prof. Henrik Alfredsson and Docent Fredrik Lundell are acknowledged. The technical and administrative staff at the department of Mechanics have been a great support.

And I greatly enjoyed the *fikas*, the lunch breaks, the afterworks, running, and *innebandy* with all my former and current coworkers, of whom Alexandra, Alexandre, Ellinor, Julie, Marco, Shahab, and Sohrab deserve a special thanks.

Lastly, I would like to thank Petra, my family, and my friends for their unconditional love and support.

References

- ABERNATHY, F. H. & KRONAUER, R. E. 1962 The formation of vortex streets. J. Fluid Mech. 13 (01), 1–20.
- ADRIAN, R. J., CHRISTENSEN, K. T. & LIU, Z.-C. 2000 Analysis and interpretation of instantaneous turbulent velocity fields. *Exp. Fluids* **29** (3), 275–290.
- Adrian, R. J. & Westerweel, J. 2011 Particle image velocimetry. Cambridge Univ Press
- AGRAWAL, A. & PRASAD, A. 2002 Properties of vortices in the self-similar turbulent jet. Exp. Fluids 33 (4), 565–577.
- Anderson, E. A. & Szewczyk, A. A. 1997 Effects of a splitter plate on the near wake of a circular cylinder in 2 and 3-dimensional flow configurations. *Exp. Fluids* **23** (2), 161–174.
- Antonia, R. A. & Fulachier, L. 1989 Topology of a turbulent boundary layer with and without wall suction. *J. Fluid Mech.* 198, 429–451.
- Antonia, R. A. & Rajagopalan, S. 1990 Determination of drag of a circular cylinder. AIAA J. 28 (10), 1833–1834.
- Antonia, R. A., Spalart, P. R. & Mariani, P. 1994 Effect of suction on the near-wall anisotropy of a turbulent boundary layer. *Phys. Fluids* 6 (1), 430–432.
- APELT, C. J. & WEST, G. S. 1975 The effects of wake splitter plates on bluff-body flow in the range $10^4 < R < 5 \times 10^4$. Part 2. J. Fluid Mech. **71** (01), 145–160.
- APELT, C. J., WEST, G. S. & SZEWCZYK, A. A. 1973 The effects of wake splitter plates on bluff-body flow in the range $10^4 < R < 5 \times 10^4$. J. Fluid Mech. **61** (01), 187–198.
- Bailey, S. C. C., Hultmark, M., Monty, J. P., Alfredsson, P. H., Chong, M. S., Duncan, R. D., Fransson, J. H. M., Hutchins, N., Marusic, I., McKeon, B. J. et al. 2013 Obtaining accurate mean velocity measurements in high Reynolds number turbulent boundary layers using pitot tubes. J. Fluid Mech. 715, 642–670.
- BALACHANDAR, S., MITTAL, R. & NAJJAR, F. M. 1997 Properties of the mean recirculation region in the wakes of two-dimensional bluff bodies. *J. Fluid Mech.* **351**, 167–199.
- Barkley, D. 2006 Linear analysis of the cylinder wake mean flow. Eur. Lett. 75 (5), 750.

- BEARMAN, P. W. 1965 Investigation of the flow behind a two-dimensional model with a blunt trailing edge and fitted with splitter plates. *J. Fluid Mech.* **21** (part 2), 241–256.
- Bearman, P. W. 1967 On vortex street wakes. J. Fluid Mech. 28, 625-641.
- Bearman, P. W. 1984 Vortex shedding from oscillating bluff bodies. *Annu. Rev. Fluid Mech.* 16 (1), 195–222.
- BEN CHIEKH, M., MICHARD, M., GROSJEAN, N. & BERA, J. C. 2004 Reconstruction temporelle dun champ aérodynamique instationnaire à partir de mesures PIV non résolues dans le temps. In *Proceedings of 9ème Congrès Francophone de Vélocimétrie Laser, 14-17 Sept., Brussels, Belgium*.
- BERGER, E. & WILLE, R. 1972 Periodic flow phenomena. Annu. Rev. Fluid Mech. 4 (1), 313–340.
- Berkooz, G., Holmes, P. & Lumley, J. L. 1993 The proper orthogonal decomposition in the analysis of turbulent flows. *Annu. Rev. Fluid Mech.* **25** (1), 539–575.
- Black, T. J. & Sarnecki, A. J. 1958 The turbulent boundary layer with suction or injection. *Tech. Rep.* 3387. Aeronautical Research Council, Reports and Memoranda.
- Bloor, M. S. 1964 The transition to turbulence in the wake of a circular cylinder. J. Fluid Mech. 19 (02), 290–304.
- Bobke, A., Örlü, R. & Schlatter, P. 2016 Simulations of turbulent asymptotic suction boundary layers. *J. Turbul.* 17 (2), 157–180.
- Brevis, W. & García-Villalba, M. 2011 Shallow-flow visualization analysis by proper orthogonal decomposition. *J. Hydraul. Res.* **49** (5), 586–594.
- Bruun, H. H. 1995 Hot-wire anemometry. Oxford University Press.
- Bull, M., Li, Y. & Pickles, J. 1995 Effects of boundary layer transition on vortex shedding from thick plates with faired leading edge and square trailing edge. In Proceedings of 12th Australasian Fluid Mechanics Conference, 10-15 Dec., Sydney, Australia, pp. 231–234.
- Buresti, G. 1998 Vortex shedding from bluff bodies. In Wind Effects on Buildings and Structures: Proceedings of the Jubileum Conference on Wind Effects on Buildings and Structures, 25-29 May, Porto Alegre, Brazil, pp. 61–96. A.A. Balkema
- Buresti, G. 2012 Elements of fluid dynamics. World Scientific.
- Buresti, G., Fedeli, R. & Ferraresi, A. 1997 Influence of afterbody rounding on the pressure drag of an axisymmetrical bluff body. *J. Wind Eng. Ind. Aerodyn.* **69**, 179–188.
- Camarri, S. 2015 Flow control design inspired by linear stability analysis. *Acta Mech.* **226** (4), 979–1010.
- Camarri, S., Fallenius, B. E. G. & Fransson, J. H. M. 2013 Stability analysis of experimental flow fields behind a porous cylinder for the investigation of the large-scale wake vortices. *J. Fluid Mech.* **715**, 499–536.
- Chauhan, K. A., Monkewitz, P. A. & Nagib, H. M. 2009 Criteria for assessing experiments in zero pressure gradient boundary layers. *Fluid Dyn. Res.* **41** (2), 021404.

- Choi, H., Jeon, W. P. & Kim, J. 2008 Control of flow over a bluff body. *Annu. Rev. Fluid Mech.* 40, 113–139.
- Chomaz, J. M., Huerre, P. & Redekopp, L. G. 1988 Bifurcations to local and global modes in spatially developing flows. *Phys. Rev. Lett.* **60**, 25–28.
- CHONG, M., PERRY, A. E. & CANTWELL, B. 1990 A general classification of three-dimensional flow fields. *Phys. Fluids A* 2 (5), 765–777.
- CHYU, C., LIN, J.-C., SHERIDAN, J. & ROCKWELL, D. 1995 Kármán vortex formation from a cylinder: Role of phase-locked Kelvin–Helmholtz vortices. *Phys. Fluids* 7 (9), 2288–2290.
- DAVIDSON, P. A. 2004 Turbulence: An Introduction for Scientists and Engineers. Oxford University Press.
- DURGESH, V., NAUGHTON, J. W. & WHITMORE, S. A. 2013 Experimental investigation of base-drag reduction via boundary-layer modification. AIAA J. 51 (2), 416–425.
- Dutton, R. 1958 The effects of distributed suction on the development of turbulent boundary layers. *Tech. Rep.* 3155. Aeronautical Research Council, Reports and Memoranda.
- FAGE, A. & JOHANSEN, F. C. 1927 On the flow of air behind an inclined flat plate of infinite span. P. Roy. Soc. Lond. A Mat. 116 (773), 170–197.
- Falkner, V. M. & Skan, S. W. 1930 Some approximate solutions of the boundary layer equations. *Tech. Rep.* 1314. Aeronautical Research Council, Reports and Memoranda.
- Fallenius, B. E. G. 2009 A new experimental setup for studies on wake flow instability and its control. *Tech. Rep.*. Royal Inst. of Technology, Dep. of Mechanics, TRITA-MEK 2009:05, Lic. Thesis.
- Fallenius, B. E. G., Trip, R. & Fransson, J. H. M. 2014 A new test section for wind tunnel studies on wake instability and its control. *Tech. Rep.*. Royal Inst. of Technology, Dep. of Mechanics, TRITA-MEK 2014:08, Technical Report.
- Fransson, J. H. M. 2010 Turbulent spot evolution in spatially invariant boundary layers. *Phys. Rev. E* 81 (3), 035301.
- Fransson, J. H. M. & Alfredsson, P. H. 2003 On the disturbance growth in an asymptotic suction boundary layer. *J. Fluid Mech.* **482**, 51–90.
- Fransson, J. H. M., Konieczny, P. & Alfredsson, P. H. 2004 Flow around a porous cylinder subject to continuous suction or blowing. *J. Fluid Struct.* **19** (8), 1031–1048.
- GERRARD, J. H. 1965 A disturbance-sensitive Reynolds number range of the flow past a circular cylinder. *J. Fluid Mech.* **22** (01), 187–196.
- GERRARD, J. H. 1966 The mechanics of the formation region of vortices behind bluff bodies. J. Fluid Mech. 25 (02), 401–413.
- GIANNETTI, F., CAMARRI, S. & LUCHINI, P. 2010 Structural sensitivity of the secondary instability in the wake of a circular cylinder. J. Fluid Mech. 651, 319.
- Giannetti, F. & Luchini, P. 2007 Structural sensitivity of the first instability of the cylinder wake. *J. Fluid Mech.* **581** (1), 167–197.
- GILLIES, E. A. 1998 Low–dimensional control of the circular cylinder wake. *J. Fluid Mech.* **371**, 157–178.

- Goldstein, S. 1938 Modern developments in fluid dynamics: an account of theory and experiment relating to boundary layers, turbulent motion and wakes. Clarendon Press.
- GOODMAN, J. W. 2005 Introduction to Fourier optics. Roberts and Company Publishers.
- GRIFFITH, A. A. & MEREDITH, F. W. 1936 The possible improvement in aircraft performance due to the use of boundary layer suction. *Tech. Rep.* E 3501. Royal Aircraft Establishment.
- GRINSTEIN, F. F., BORIS, J. P. & GRIFFIN, O. M. 1991 Passive pressure-drag control in a plane wake. AIAA J. 29, 1436–1442.
- Hammond, D. A. & Redekopp, L. G. 1997 Global dynamics of symmetric and asymmetric wakes. *J. Fluid Mech.* **331**, 231–260.
- HANNEMANN, K. & OERTEL, H. 1989 Numerical simulation of the absolutely and convectively unstable wake. J. Fluid Mech. 199, 55–88.
- HOERNER, S. F. 1965 Fluid-dynamic drag: practical information on aerodynamic drag and hydrodynamic resistance. Hoerner Fluid Dynamics Midland Park, NJ.
- Hu, J. C., Zhou, Y. & Dalton, C. 2006 Effects of the corner radius on the near wake of a square prism. *Exp. Fluids* **40** (1), 106–118.
- Huerre, P. & Monkewitz, P. A. 1990 Local and global instabilities in spatially developing flows. *Annu. Rev. Fluid Mech.* **22**, 473–537.
- HUTCHINS, N., NICKELS, T. B., MARUSIC, I. & CHONG, M. S. 2009 Hot-wire spatial resolution issues in wall-bounded turbulence. *J. Fluid Mech.* **635**, 103–136.
- JEONG, J. & HUSSAIN, F. 1995 On the identification of a vortex. J. Fluid Mech. 285, 69–94.
- Jodai, Y., Takahashi, Y., Ichimiya, M. & Osaka, H. 2008 The effects of splitter plates on turbulent boundary layer on a long flat plate near the trailing edge. *J. Fluids Eng.* **130** (5).
- JOHANSSON, A. V. & ALFREDSSON, P. H. 1982 On the structure of turbulent channel flow. J. Fluid Mech. 122, 295–314.
- KAY, J. M. 1948 Boundary-layer flow along a flat plate with uniform suction. *Tech. Rep.* 2628. Aeronautical Research Council, Reports and Memoranda.
- Khapko, T. 2014 Transition to turbulence in the asymptotic suction boundary layer. *Tech. Rep.*. Royal Inst. of Technology, Dep. of Mechanics, TRITA-MEK 2014:03, Lic. Thesis.
- KHOR, M., SHERIDAN, J., THOMPSON, M. C. & HOURIGAN, K. 2008 Global frequency selection in the observed time-mean wakes of circular cylinders. J. Fluid Mech. 601, 425–441.
- KIM, W., YOO, J. Y. & SUNG, J. 2006 Dynamics of vortex lock-on in a perturbed cylinder wake. Phys. Fluids 18 (7), 074103.
- Kostas, J., Soria, J. & Chong, M. 2002 Particle image velocimetry measurements of a backward-facing step flow. *Exp. Fluids* **33** (6), 838–853.
- Kumar, R. A., Sohn, C. H. & Gowda, B. H. L. 2015 A PIV study of the near wake flow features of a square cylinder: influence of corner radius. *J. Mech. Sci. Technol.* **29** (2), 527–541.
- Kundu, P. K. & Cohen, I. M. 2008 Fluid Mechanics. Elsevier Academic Press.

- LEONTINI, J. S., THOMPSON, M. C. & HOURIGAN, K. 2010 A numerical study of global frequency selection in the time-mean wake of a circular cylinder. *J. Fluid Mech.* **645** (1), 435–446.
- LINDGREN, B. 2002 Flow facility design and experimental studies of wall-bounded turbulent shear-flows. *Tech. Rep.*. Royal Inst. of Technology, Dep. of Mechanics, TRITA-MEK 2002:16, PhD Thesis.
- MALKUS, W. V. R. 1956 Outline of a theory of turbulent shear flow. *J. Fluid Mech.* 1 (05), 521–539.
- Mantič-Lugo, V., Arratia, C. & Gallaire, F. 2014 Self-consistent mean flow description of the nonlinear saturation of the vortex shedding in the cylinder wake. *Phys. Rev. Lett.* **113** (084501).
- MARIOTTI, A. & BURESTI, G. 2013 Experimental investigation on the influence of boundary layer thickness on the base pressure and near-wake flow features of an axisymmetric blunt-based body. *Exp. Fluids* **54** (11), 1–16.
- MARQUET, O., SIPP, D. & JACQUIN, L. 2008 Sensitivity analysis and passive control of cylinder flow. *J. Fluid Mech.* **615**, 221–252.
- MATHELIN, L., BATAILLE, F. & LALLEMAND, A. 2001a Near wake of a circular cylinder submitted to blowing–I: boundary layers evolution. *Int. J. Heat Mass Transf.* 44 (19), 3701–3708.
- Mathelin, L., Bataille, F. & Lallemand, A. 2001b Near wake of a circular cylinder submitted to blowing–II: impact on the dynamics. *Int. J. Heat Mass Transf.* 44 (19), 3709–3719.
- McKeon, B. J., Li, J., Jiang, W., Morrison, J. F. & Smits, A. J. 2003 Pitot probe corrections in fully developed turbulent pipe flow. *Meas. Sci. Technol.* 14, 1449.
- Meliga, P., Pujals, G. & Serre, É. 2012 Sensitivity of 2-D turbulent flow past a D-shaped cylinder using global stability. *Phys. Fluids* **24**, 061701.
- MITTAL, S. 2008 Global linear stability analysis of time-averaged flows. Int. J. Numer. Methods Fluids $\bf 58$ (1), 111-118.
- Monkewitz, P. A. 1988 The absolute and convective nature of instability in two-dimensional wakes at low Reynolds numbers. *Phys. Fluids* **31** (5), 999–1006.
- Monkewitz, P. A., Huerre, P. & Chomaz, J.-M. 1993 Global linear stability analysis of weakly non-parallel shear flows. *J. Fluid Mech.* **251**, 1–20.
- NAGHIB-LAHOUTI, A., LAVOIE, P. & HANGAN, H. 2014 Wake instabilities of a blunt trailing edge profiled body at intermediate Reynolds numbers. *Exp. Fluids* **55** (7), 1–15.
- NAGIB, H. M., CHAUHAN, K. A. & MONKEWITZ, P. A. 2007 Approach to an asymptotic state for zero pressure gradient turbulent boundary layers. *Phil. Trans. R. Soc. A* **365** (1852), 755–770.
- NAKAMURA, Y. 1996 Vortex shedding from bluff bodies with splitter plates. *J. Fluids Struc.* 10, 147–158.
- NICKELS, T. B. 2004 Inner scaling for wall-bounded flows subject to large pressure gradients. *J. Fluid Mech.* **521**, 217–239.
- Noack, B. R., Afanasiev, K., Morzynski, M., Tadmor, G. & Thiele, F. 2003 A

- hierarchy of low-dimensional models for the transient and post-transient cylinder wake. J. Fluid Mech. 497, 335–363.
- NORBERG, C. 1987 Effects of Reynolds number and a low-intensity freestream turbulence on the flow around a circular cylinder. *Tech. Rep.* 87/2. Chalmers University of Technology, Department of Applied Thermodynamics and Fluid Mechanics.
- NORBERG, C. 1994 An experimental investigation of the flow around a circular cylinder: influence of aspect ratio. *J. Fluid Mech.* **258**, 287–316.
- NORBERG, C. 2003 Fluctuating lift on a circular cylinder: review and new measurements. J. Fluids Struc. 17, 57–96.
- Ozono, S. 1999 Flow control of vortex shedding by a short splitter plate asymmetrically arranged downstream of a cylinder. *Phys. Fluids* **11**, 2928–2934.
- Parezanović, V. & Cadot, O. 2009 The impact of a local perturbation on global properties of a turbulent wake. *Phys. Fluids* **21** (7), 071701.
- Parezanović, V. & Cadot, O. 2012 Experimental sensitivity analysis of the global properties of a two-dimensional turbulent wake. J. Fluid Mech. 1 (1), 1–35.
- Parker, R. & Welsh, M. C. 1983 Effects of sound on flow separation from blunt flat plates. *Int. J. Heat Fluid Flow* 4 (2), 113–127.
- Pastoor, M., Henning, L., Noack, B. R., King, R. & Tadmor, G. 2008 Feedback shear layer control for bluff body drag reduction. *J. Fluid Mech.* **608**, 161–196.
- Perrin, R., Braza, M., Cid, E., Cazin, S., Barthet, A., Sevrain, A., Mockett, C. & Thiele, F. 2007 Obtaining phase averaged turbulence properties in the near wake of a circular cylinder at high Reynolds number using POD. *Exp. Fluids* 43 (2-3), 341–355.
- Petrusma, M. & Gai, S. 1994 The effect of geometry on the base pressure recovery of segmented blunt trailing edges. *Aeronaut. J.* **98** (977), 267–274.
- PIER, B. 2002 On the frequency selection of finite-amplitude vortex shedding in the cylinder wake. *J. Fluid Mech.* **458**, 407–417.
- Pol, S., Hoffman, J. & Balasubramaniam, B. 2011 Large field of view particle-image velocimetry (LF-PIV): Design and performance. *Bull. Am. Phys. Soc.* 56.
- Poll, D., Danks, M. & Humphreys, B. 1992 The aerodynamic performance of laser drilled sheets. In *First European Forum on Laminar Flow Technology*, 16-18 March, Hamburg, Germany, pp. 274–277.
- Pope, S. B. 2000 Turbulent flows. Cambridge University Press.
- Prandtl, L. 1904 Über flüssigkeitsbewegung bei sehr kleiner reibung. In Verhandlungen des dritten Internationalen Mathematiker-kongresses, 8-13 Aug., Heidelberg, Germany, pp. 484–491.
- PROVANSAL, M., MATHIS, C. & BOYER, L. 1987 Bénard-von Kármán instability: transient and forced regimes. *J. Fluid Mech.* **182**, 1–22.
- RAFFEL, M., WILLERT, C. E., WERELEY, S. T. & KOMPENHANS, J. 2007 Particle Image Velocimetry A practical guide, 2nd edn. Springer-Verlag.
- RANGA RAJU, K. G., POREY, P. D. & ASAWA, G. L. 1997 Displacement effect in pitot tube measurements in shear flows. *J. Wind Eng. Ind. Aerod.* **66** (2), 95–105.
- RAYLEIGH, J. W. S. 1878 The theory of sound, 2nd edn., p. 413. MacMillan and

- CO., LTD, Reprint (1945) from the collections of the University of California Llibraries.
- Reau, N. & Tumin, A. 2002 On harmonic perturbations in a turbulent mixing layer. Eur. J. Mech. - B/Fluids 21 (2), 143–155.
- Rehimi, F., Aloui, F., Nasrallah, S. B., Doubliez, L. & Legrand, J. 2008 Experimental investigation of a confined flow downstream of a circular cylinder centred between two parallel walls. *J. Fluid Struct.* **24** (6), 855–882.
- REYNOLDS, W. C. & HUSSAIN, A. K. M. F. 1972 The mechanics of an organized wave in turbulent shear flow. Part 3. Theoretical models and comparisons with experiments. *J. Fluid Mech.* **54** (02), 263–288.
- RHEINBOLDT, W. 1955 Zur Berechnung stationärer Grenzschichten bei kontinuierlicher Absaugung mit unstetig veränderlicher Absaugegeschwindigkeit. *Tech. Rep.*. Albert-Ludwigs-University, PhD Thesis, [Translation: The calculation of steady boundary layers for continuous suction, with discontinuously variable suction velocity, 1961, NASA TT F-29].
- RICHTER, A. & NAUDASCHER, E. 1976 Fluctuating forces on a rigid circular cylinder in confined flow. *J. Fluid Mech.* **78** (03), 561–576.
- ROSENHEAD, L. 1963 Laminar Boundary Layers: An Account of the Development, Structure, and Stability of Laminar Boundary Layers in Incompressible Fluids, Together with a Description of the Associated Experimental Techniques. Clarendon Press.
- ROSHKO, A. 1953 On the development of turbulent wakes from vortex streets. Tech. Rep. NACA TN 2913. National Advisory Committee for Aeronautics.
- ROSHKO, A. 1954 On the drag and shedding frequency of two-dimensional bluff bodies. *Tech. Rep.* NACA TN 3169. National Advisory Committee for Aeronautics.
- ROSHKO, A. 1955 On the wake and drag of bluff bodies. J. Aeronaut. Sci. 22, 124–132.
- ROSHKO, A. 1961 Experiments on the flow past a circular cylinder at very high Reynolds number. J. Fluid Mech. 10 (03), 345–356.
- ROSHKO, A. 1993 Free shear layers, base pressure and bluff-body drag. In *Proceedings* of the Symposium on Developments in Fluid Dynamics and Aerospace Engineering, 9-10 Dec, Bangalore, India.
- ROTTA, J. C. 1970 Control of turbulent boundary layers by uniform injection and suction of fluid. Jahrbuch 1970 der Deutsche Gesellschaft für Luft- und Raumfahrt E.V. (DGLR) pp. 91–104.
- ROWE, A., FRY, A. L. A. & MOTALLEBI, F. 2001 Influence of boundary layer thickness on base pressure and vortex shedding frequency. *AIAA J.* **39** (4).
- Santa Cruz, A., David, L., Pecheux, J. & Texier, A. 2005 Characterization by proper-orthogonal-decomposition of the passive controlled wake flow downstream of a half cylinder. *Exp. Fluids* **39** (4), 730–742.
- SARIC, W. S., REED, H. L. & KERSCHEN, E. J. 2002 Boundary-layer receptivity to freestream disturbances. *Annu. Rev. Fluid Mech.* **34**, 291–319.
- Scarano, F. & Riethmuller, M. L. 2000 Advances in iterative multigrid PIV image processing. *Exp. Fluids* **29** (1), S051–S060.
- SCHILLER, L. & LINKE, W. 1933 Druck- und Reibungswiderstand des Zylinders bei

- Reynoldsschen Zahlen 5000 bis 40000. Zeitschrift für Flugtechnik und Motorluftschiffahrt 24 (7), 193–198, [Translation: Pressure and frictional resistance of a cylinder at Reynolds numbers 5000 to 40000, 1933, National Advisory Committee for Aeronautics NACA TM 715].
- Schlatter, P. & Örlü, R. 2011 Turbulent asymptotic suction boundary layers studied by simulation. In *J. Phys. Conf. Ser.*, 13th European Turbulence Conference (ETC13), 12-15 Sept., Warsaw, Poland, vol. 318, p. 022020. IOP Publishing.
- SIEVERDING, C. & HEINEMANN, H. 1990 The influence of boundary layer state on vortex shedding from flat plates and turbine cascades. *J. Turbomach.* **112** (2), 181–187.
- SIMPSON, R. L. 1970 Characteristics of turbulent boundary layers at low Reynolds numbers with and without transpiration. *J. Fluid Mech.* **42** (04), 769–802.
- SIMPSON, R. L., MOFFAT, R. J. & KAYS, W. M. 1969 The turbulent boundary layer on a porous plate: experimental skin friction with variable injection and suction. *Int. J. Heat Mass Transf.* **12** (7), 771–789.
- SIPP, D. & LEBEDEV, A. 2007 Global stability of base and mean flows: a general approach and its applications to cylinder and open cavity flows. *J. Fluid Mech.* **593**, 333–358.
- SIROVICH, L. 1987 Turbulence and the dynamics of coherent structures. part I: Coherent structures. Q. Appl. Math. 45 (3), 561–571.
- SMITS, A. J., MATHESON, N. & JOUBERT, P. N. 1983 Low-Reynolds-number turbulent boundary layers in zero and favorable pressure gradients. *J. Ship Res.* 27 (3), 147–157.
- SPALART, P. R. & ALLMARAS, S. R. 1994 One-equation turbulence model for aero-dynamic flows. *Rechearche Aerosp.* 1, 5–21.
- SREENIVASAN, K. R., STRYKOWSKI, P. J. & OLINGER, D. J. 1987 Hopf bifurcation, Landau equation, and vortex shedding behind circular cylinders. In Forum on unsteady flow separation, The 1987 ASME Applied Mechanics, Bioengineering, and Fluids Engineering Conference, 14-17 June, Cincinnati, Ohio, USA, pp. 1–13. The American Society of Mechanical Engineers (ASME).
- Strouhal, V. 1878 Über eine besondere art der tonerregung. Annalen der Physik **241** (10), 216–251.
- STRYKOWSKI, P. J. & SREENIVASAN, K. R. 1990 On the formation and suppression of vortex shedding at low Reynolds numbers. *J. Fluid Mech.* 218, 71–107.
- Sychev, V. V. 1982 Asymptotic theory of separation flows. Fluid Dynamics 17 (2), 179–188.
- Taylor, Z. J., Palombi, E., Gurka, R. & Kopp, G. A. 2011 Features of the turbulent flow around symmetric elongated bluff bodies. *J. Fluid Struct.* 27 (2), 250–265.
- Tennekes, H. 1965 Similarity laws for turbulent boundary layers with suction or injection. J. Fluid Mech. 21 (part 4), 689–703.
- TRIP, R. & FRANSSON, J. H. M. 2014 Boundary layer modification by means of wall suction and the effect on the wake behind a rectangular forebody. *Phys. Fluids* **26** (12), 125105.

- TRIP, R. & FRANSSON, J. H. M. 2015 An experimental study on the relation between the wake inlet conditions and the near wake topology. In *Proceedings of International Conference on Jets, Wakes and Separated Flows (ICJWSF 2015)*, 15-18 June, Stockholm, Sweden. To be published.
- TRIP, R. & Fransson, J. H. M. 2016 On the effect of boundary layer modification on the near-wake topology of a rectangular forebody. Paper 5, Manuscript.
- TROPEA, C., Yarin, A. L. & Foss, J. F. 2007 Springer handbook of experimental fluid mechanics. Springer.
- UNAL, M. F. & ROCKWELL, D. 1988 On vortex formation from a cylinder. Part 2. control by splitter-plate interference. *J. Fluid Mech* **190**, 513–529.
- Van Driest, E. 1956 On turbulent flow near a wall. J. Aeronaut. Sci. 23 (11), 1007-1011.
- Van Oudheusden, B., Scarano, F., Van Hinsberg, N. & Watt, D. 2005 Phase-resolved characterization of vortex shedding in the near wake of a square-section cylinder at incidence. *Exp. Fluids* **39** (1), 86–98.
- VIOLA, F., IUNGO, G. V., CAMARRI, S., PORTÉ-AGEL, F. & GALLAIRE, F. 2014 Prediction of the hub vortex instability in a wind turbine wake: stability analysis with eddy-viscosity models calibrated on wind tunnel data. J. Fluid Mech. 750, R1.
- Von Kármán, T. & Rubach, H. 1912 Uber den mechanismus des flüssigkeits und luftwiderstandes. *Physikalische Zeitschrift* **13** (2), 49–59, [Translation: On the resistance mechanisms of fluids and air, 1975, NASA TT F-16, 415].
- Wang, C. Y. 2011 Review of similarity stretching exact solutions of the Navier–Stokes equations. Eur. J. Mech. B/Fluids 30 (5), 475–479.
- Wei, T. & Smith, C. R. 1986 Secondary vortices in the wake of circular cylinders. J. Fluid Mech. 169, 513–533.
- West, G. & Apelt, C. 1982 The effects of tunnel blockage and aspect ratio on the mean flow past a circular cylinder with Reynolds numbers between 10⁴ and 10⁵.

 J. Fluid Mech. 114, 361–377.
- Westerweel, J. & Scarano, F. 2005 Universal outlier detection for PIV data. Exp. Fluids 39 (6), 1096–1100.
- WILLIAMSON, C. H. K. 1989 Oblique and parallel modes of vortex shedding in the wake of a circular cylinder at low Reynolds numbers. J. Fluid Mech. 206, 579– 627.
- WILLIAMSON, C. H. K. 1996 Vortex dynamics in the cylinder wake. Annu. Rev. Fluid Mech. 28 (1), 477–539.
- WOOD, C. J. 1967 Visualization of an incompressible wake with base bleed. J. Fluid Mech. 29 (02), 259–272.
- Yoshioka, S., Fransson, J. H. M. & Alfredsson, P. H. 2004 Free stream turbulence induced disturbances in boundary layers with wall suction. *Phys. Fluids* 16, 3530.
- Yucel, S. B., Cetiner, O. & Unal, M. F. 2010 Interaction of circular cylinder wake with a short asymmetrically located downstream plate. *Exp. Fluids* **49** (1), 241–255.

- ZDRAVKOVICH, M. M. 1981 Review and classification of various aerodynamic and hydrodynamic means for suppressing vortex shedding. *J. Wind Eng. Ind. Aerodyn.* 7 (2), 145–189.
- ZDRAVKOVICH, M. M. 1997 Flow around Circular Cylinders: Volume 1: Fundamentals. Oxford University Press.
- ZDRAVKOVICH, M. M. 2003 Flow around circular cylinders, Volume 2: Applications. Oxford University Press.
- Zhou, J. Adrian, R. J., Balachandar, S. & Kendall, T. M. 1999 Mechanisms for generating coherent packets of hairpin vortices in channel flow. *J. Fluid Mech.* **387**, 353–396.
- Zhou, Y. & Antonia, R. A. 1993 A study of turbulent vortices in the near wake of a cylinder. J. Fluid Mech. 253, 643–661.

Part II

Papers